

INVESTIGATION OF CARBOXYL-FUNCTIONALIZED SELF-ASSEMBLED  
MONOLAYERS ON GOLD SURFACES

A THESIS SUBMITTED TO  
THE GRADUATE SCHOOL OF NATURAL AND APPLIED SCIENCES  
OF  
MIDDLE EAST TECHNICAL UNIVERSITY

BY

SALIHA GÖRGÜLÜ

IN PARTIAL FULFILLMENT OF THE REQUIREMENTS  
FOR  
THE DEGREE OF MASTER OF SCIENCE  
IN  
CHEMISTRY

JANUARY 2020

Approval of the thesis:

**INVESTIGATION OF CARBOXYL-FUNCTIONALIZED SELF-  
ASSEMBLED MONOLAYERS ON GOLD SURFACES**

submitted by **SALIHA GÖRGÜLÜ** in partial fulfillment of the requirements for  
the degree of **Master of Science in Chemistry Department, Middle East  
Technical University** by,

Prof. Dr. Halil Kalıpçılar

Dean, Graduate School of **Natural and Applied Sciences**

---

Prof. Dr. Cihangir Tanyeli

Head of Department, **Chemistry**

---

Assoc. Prof. Dr. Mehmet Fatih Danışman

Supervisor, **Chemistry, METU**

---

**Examining Committee Members:**

Prof. Dr. Mürvet Volkan

Chemistry Dept., METU

---

Assoc. Prof. Dr. Mehmet Fatih Danışman

Chemistry, METU

---

Assoc. Prof. Dr. Gülay Ertuş

Chemistry Dept., METU

---

Assoc. Prof. Dr. İrem Erel Göktepe

Chemistry Dept., METU

---

Assoc. Prof. Dr. Gökçen Birlik Demirel

Chemistry Dept., Ankara Hacı Bayram Veli Univ.

---

Date: 15.01.2020

**I hereby declare that all information in this document has been obtained and presented in accordance with academic rules and ethical conduct. I also declare that, as required by these rules and conduct, I have fully cited and referenced all material and results that are not original to this work.**

Name, Surname: Saliha Görgülü

Signature:

## ABSTRACT

### INVESTIGATION OF CARBOXYL-FUNCTIONALIZED SELF-ASSEMBLED MONOLAYERS ON GOLD SURFACES

Görgülü, Saliha  
Master of Science, Chemistry  
Supervisor: Assoc. Prof. Dr. Mehmet Fatih Danişman

January 2020, 78 pages

Thiolated derivatives of dicarba-closo-dodecaborane, HS-C<sub>2</sub>B<sub>10</sub>H<sub>11</sub> (carboranethiol, CT), with icosahedral molecular structure are one of the promising candidates for self-assembled monolayer (SAM) applications. CT SAMs possess various advantages relative to their organic counterparts, such as high stability towards chemical, oxidative and thermal degradations as well as having fewer defects. In this study unfunctionalized CT SAMs (M1, M9) and carboxylic group functionalized CT SAMs (M1C, M9C) as well as their corresponding mixed SAMs were investigated on template stripped gold surfaces. Wetting properties of the SAMs were studied by using contact angle (CA) measurements. The ellipsometric thickness of all SAMs were found to be about 1-2 nm which is consistent with the reported thickness, measured by scanning tunneling microscopy (STM), in the literature. In mixed SAMs, surface fraction of M1 was found to be higher than its solution fraction in the M1:M1C and M1:M9C mixtures indicating the dominant component on the surface

to be M1. Similar behavior was also observed for M9 such that surface fraction of M9 was higher than its solution fraction in the M9:M1C and M9:M9C mixtures indicating the dominance of M9 molecules on the surface. M1 and M9 molecules bind to gold surface stronger than M1C and M9C molecules. In replacement experiments of CT SAMs, M1 molecules were found to replace M9C faster than M9C replaces M1 on template stripped gold surface. Replacement experiments of CT SAMs on silver surface were also performed. It was found that M9C molecules bind to silver surfaces through carboxylic groups rather than the thiol group.

Keywords: Carboranethiol, Self-Assembled monolayers, Gold surfaces, Contact angle.

## ÖZ

### **KARBOKSİL FONKSİYONEL GRUP BAĞLANMIŞ KARBORANTİYOL KENDİLİĞİNDEN DÜZENLENEN TEK KATMANLI YAPILARIN (KDT) ALTIN YÜZEY ÜZERİNDEKİ DAVRANIŞLARININ İNCELENMESİ**

Görgülü, Saliha  
Yüksek Lisans, Kimya  
Tez Danışmanı: Doç. Dr. Mehmet Fatih Danışman

Ocak 2020, 78 sayfa

İkozahedral moleküler yapıya sahip tiyol türevi olan karborantiyoller ( $HS-C_2B_{10}H_{11}$ , KT), kendiliğinden düzenlenmiş tek-tabaka (KDT) uygulamaları için ümit vaat etmektedir. KT izomerlerinin, özdeş geometrik yapıya sahip olmaları sayesinde, KDT uygulamalarında birçok üstünlükleri bulunmaktadır. KT KDT'ler organik emsallerine göre kimyasal ve termal bozulmaya ve oksitlenmeye karşı daha dirençli olup daha az kusur içermektedirler. Bu çalışmada karborantiyollerin fonksiyonel grup içermeyen (M1, M9) ve karboksil fonksiyonel grubu içeren (M1C, M9C) karışım filmleri sıyrılmış altın yüzeyler üzerinde incelenmiştir. KDT'lerin genel özellikleri temas açısı ve spektroskopik elipsometri ölçümleri ile karakterize edilmişlerdir. KDT'lerin elipsometrik kalınlıkları yaklaşık 1-2 nm aralığında bulunmuştur ve bu sonuç literatürdeki, tünelleme tarama mikroskobu (STM) ölçümleri ile elde edilen kalınlık değerleri ile örtüşmektedir. KT KDT'lerin karışım deneylerinde, M1 ve M9 moleküllerinin M1C ve M9C moleküllerine göre sıyrılmış

altın yüzeye daha sıkı tutunduğu bulunmuştur. M1:M1C ve M1:M9C karışımları için M1'in yüzey fraksiyonunun M1'in çözelti fraksiyonundan yüksek olduğu bulunmuştur bu da yüzeydeki baskın bileşenin M1 molekülü olduğunu göstermektedir. Benzer davranış M9:M1C ve M9:M9C karışımları için de gözlemlenmiştir. M9'un yüzey fraksiyonunun M9'un çözelti fraksiyonundan yüksek olduğu bulunmuştur ki bu da yüzeydeki baskın bileşenin M9 molekülü olduğunu göstermiştir. Sıyrılmış altın yüzey üzerindeki yer değiştirme deneylerinde M1 molekülerinin M9C molekülleri ile yer değiştirme hızının, M9C molekülerinin M1 molekülleri ile yer değiştirme hızından daha fazla olduğu bulunmuştur. Sıyrılmış gümüş yüzey üzerindeki yer değiştirme deneylerinde ise M9C moleküllerinin yüzeye kükürt üzerinden değil karboksilik grubundaki oksijen üzerinden bağlandığı bulunmuştur.

Anahtar Kelimeler: Karborantiyol, KDT, Altın yüzey, Temas açısı.

To my husband

## ACKNOWLEDGEMENTS

I would like to indicate my extreme gratitude to my thesis supervisor Assoc. Prof. Dr. Mehmet Fatih Danışman. I owe thanks to him for endless efforts, precious feedback, patience and encouragements during my thesis study. I would like to thank all jury members not only for their time and patience, but also helping me improve this thesis significantly with their valuable comments. My special thanks go to Adem Yavuz for helping me during this study and sharing his experience as well as experiments results.

I would like to thank Assoc. Prof. Gülay Ertaş for valuable contribution to XPS analysis. I would like to thank Assoc. Prof. Salih Özçubukçu for valuable contribution to our discussion about Carboxylated CTs. I thank The Center for Solar Energy Research and Applications (GÜNAM) and Prof. Dr. Levent Toppare for letting us use their thermal evaporator for gold film growth and Mertcan Erer for helping us using the evaporator. I thank Dr. Tomas Base at the Institute of Inorganic Chemistry, the Czech Academy of Sciences for providing the carboxyl functionalized carboranethiols. This work was very partially supported by METU-BAP project no LT-103-2018-3684.

I would like to express my sincere thanks to my friends who support me during master program Merve Canyurt, Emine Ayşe Turhan, Merve Derya Oflaz. I would like to thank my family for their love and support during my whole life. And to Kazım, his endless support, encouragement and patience made me to do my best.

## TABLE OF CONTENTS

ABSTRACT .....	v
ÖZ .....	vii
ACKNOWLEDGEMENTS .....	x
TABLE OF CONTENTS .....	xi
LIST OF TABLES .....	xiv
LIST OF FIGURES .....	xv
LIST OF ABBREVIATIONS .....	xix
CHAPTERS	
1. INTRODUCTION .....	1
1.1. Background .....	1
1.2. Concept of Self-Assembly.....	3
1.2.1. Headgroup.....	3
1.2.2. Molecular Backbone .....	4
1.2.3. Terminal Group.....	5
1.3. Mechanism and Kinetics of SAM formation .....	6
1.3.1. SAM Formation .....	6
1.3.1.1. Solution-phase monolayer formation.....	6
1.3.1.2. Gas phase monolayer formation.....	7
1.4. Characterization of Thiol SAMs .....	8
1.5. Carboranethiol (CT) SAMs .....	11
1.6. Motivation of Study.....	17
2. EXPERIMENTAL.....	19

2.1. Characterization Techniques.....	19
2.1.1. Atomic Force Microscopy (AFM) .....	19
2.1.2. Spectroscopic Ellipsometry (SE).....	21
2.1.3. Contact Angle.....	24
2.1.3.1. Static contact angle .....	25
2.1.3.2. Dynamic contact angle .....	26
2.1.4. X-Ray photo-electron spectroscopy (XPS) .....	27
2.2. Specific Experimental Procedure.....	29
2.2.1. Materials.....	29
2.2.2. SAM preparation .....	32
2.2.3. Template stripped (TS) gold and silver film preparation .....	32
2.2.4. Contact angle.....	34
2.2.5. Spectroscopic ellipsometry.....	35
2.2.6. Atomic force microscopy .....	36
2.2.7. X-Ray Photoelectron Spectroscopy.....	36
3. RESULTS AND DISCUSSION .....	37
3.1. Pure carboranethiol self-assembled monolayers.....	37
3.2. Mixed carboranethiol self-assembled monolayers.....	38
3.2.1. M1:M1C and M1:M9C mixed CT SAMs .....	39
3.2.2. M9:M9C mixed CT SAMs.....	45
3.2.3. M9:M1C mixed CT SAMs.....	47
3.3. Replacement Experiments.....	51
3.3.1. M1 films in M9C solution and M9C films in M1 solution .....	52
3.3.2. M9 films in M1C solution.....	56

3.3.3. M1C films in M9 solution .....	58
3.4. Replacement Experiments on Ag surfaces .....	59
3.4.1. M1 films in M9C solution and M9C films in M1 solution.....	60
3.4.2. M9 films in M1C solution and M1C films in M9 solution.....	61
3.5. X-Ray photoelectron spectroscopy results .....	62
4. CONCLUSION.....	67
REFERENCES.....	69
APPENDICES	
A. Raw Data of XPS Measurements .....	77

## LIST OF TABLES

### TABLES

Table 1.1 Contact angle of Carboranthiol of M1, M9 and M1:M9 mixed SAMs. ....	15
Table 3.1 Contact angles of carboxylated and pure carboranethiol SAMs. Literature values from reference [99] are given in parenthesis. ....	38
Table 3.2 Contact angles of M1:M1C mixed SAMs .....	41
Table 3.3 Contact angles of M1:M9C mixed SAMs .....	43
Table 3.4 Contact angles of M9:M9C mixed SAMs .....	46
Table 3.5 Contact angles of M9:M1C mixed SAMs .....	48
Table 3.6 Contact angles of M1 films in M9C solution replacement experiment. ....	54
Table 3.7 Contact angles of M9C films in M1 solution replacement experiment. ....	55
Table 3.8 Contact angles of M9 films in M1C solution replacement experiment. ....	57
Table 3.9 Contact angles of M1C films in M9 solution replacement experiment. ....	59
Table 3.10 Measured Core Level Binding Energies and FWHM of M9C films in M1 solution. ....	66
Table 3.11 Atomic Concentrations of Elements on Au Surfaces Relative to the Concentration of Boron Atoms (=10) As Determined from XPS Analyses Assuming Homogeneous Samples. ....	66

## LIST OF FIGURES

### FIGURES

Figure 1-1 Overview of various preparation routes of organic thin films. Retrieved from ref [6].	2
Figure 1-2 Schematic diagram shows the constituents of a SAM-molecule. Retrieved from ref [43].	3
Figure 1-3 The different absorption sites on Au (111). Grey dot represents “top” site, red dot indicates a bridge site and blue one corresponds to a hollow site (hcp or fcc).	4
Figure 1-4 Scheme of the different steps taking place during the self-assembly of alkanethiol on Au(111): (i) physisorption, (ii) lying down phase formation, (iii) nucleation of the standing up phase, (iv) completion of the standing up phase. Retrieved from ref [5].	8
Figure 1-5 Ellipsometric thickness of SAMs. Line indicates calculated theoretical thickness. Retrived from ref [35].	10
Figure 1-6 AFM image of bare Au(111) with hexagonal structure. b) AFM image Octadecanethiol on gold surface. Hexagonal structure of SAM is shown by vectors. c) AFM image of decanethiol. d) AFM image of hexanethiol. Retrieved from ref [96].	11
Figure 1-7 Chemical structures of M1 and M9 carboranethiols. Grey: carbon, pink: boron, yellow: sulphur, white: hydrogen.	12
Figure 1-8 Dipole moment direction of M1 and M9. Retrieved from [99].	13
Figure 1-9 STM images of SAMs of A) M1. B) M9 and C) an adlayer prepared from a 1:1 solution on gold surface. Inset in A and B correspond to fourier transforms image A and B showing reciprocal lattice. Retrieved from ref [99].	13
Figure 1-10 Head to tail dipole moment of M1 and perpendicular dipole of M9. Retrieved from ref [99].	14
Figure 1-11 Chemical structure of A and A'. Retrieved from ref [102].	15

Figure 1-12 I) STM images of A. II) Observed lattice, blue lines indicates nearest neighbors. III) Mixed 1:10, A', A SAM. IV) Thresholding enables the isolation of A' regions that are highlighted in red. Retrieved from ref[102].	16
Figure 1-13 X-ray photoelectron spectrum of S 2p photoelectrons fit to indicate the contributions of both the thiolate (green) and the thiol (yellow) bound moieties of A' on gold surfaces. Retrieved from ref[102].	17
Figure 1-14 Four different carboranethiol molecules studied in this thesis. Grey:Carbon, Pink:Boron, Yellow:Sulfur, Red:Oxygen, White:Hydrogen.	18
Figure 2-1 Schematic illustration of AFM working principle. Retrieved from [ref 99].	20
Figure 2-2 Illustrative force vs distance curve between the scanning tip and sample. Retrieved from ref [98].	20
Figure 2-3 The working principle of spectroscopic ellipsometry. Retrieved from ref [96].	23
Figure 2-4 Experimentally measured data fitted with models A) Fitted template stripped gold film by using Drude Lorenz dielectric function and gold/air two phase model. B) Fitted carboranethiol film by using the reference gold parameters, Cauchy dielectric function for SAM and gold/Sam/air three phase model. Retrieved from ref [98].	23
Figure 2-5 Young's construction of the force balance at a three phase contact line between a droplet, its vapor, and a solid surface. Retrieved from ref [5].	24
Figure 2-6 Static contact angle of 1-Octadecanethiol SAM on thermally evaporated gold on mica.	26
Figure 2-7 Illustration of advancing and receding angle. Retrieved from ref [99].	27
Figure 2-8 Schematic diagram of photoelectron spectroscopy. Retrieved from ref [101].	29
Figure 2-9 Scheme of general experimental procedure.	31
Figure 2-10 A) AFM images of thermally evaporated gold on mica. B) AFM image of TS gold film. Retrieved from ref [98]	33
Figure 2-11 Illustration of template stripped gold surface preparation procedure.	34

Figure 3-1 Contact angles and ellipsometric thickness for pure and carboxylated carboranethiols. S: static, A: advancing and R: receding contact angles.....	37
Figure 3-2 Contact angles and ellipsometric thicknesses of M1:M1C mixed SAMs as a function of growth solution mole ratio of M1 to M1C. S: static, A: advancing and R: receding contact angles .....	40
Figure 3-3 Surface composition of mixed M1:M1C SAMs calculated from the observed contact angles, plotted as a function of growth solution composition. S: static, A: advancing and R: receding contact angles.....	41
Figure 3-4 AFM images M1:M1C (1:1) mixed SAMs on template stripped gold surface. (1.25x1.25 $\mu\text{m}^2$ ).....	42
Figure 3-5 Contact angles and ellipsometric thicknesses of M1:M9C mixed SAMs. S: static, A: advancing and R: receding contact angles.....	43
Figure 3-6 Surface composition of mixed M1:M9C SAMs calculated from the observed contact angles, plotted as a function of growth solution composition. S: static, A: advancing and R: receding contact angles.....	44
Figure 3-7 AFM images M1:M9C (1:1) mixed SAMs on template stripped gold surface. (1.25x1.25 $\mu\text{m}^2$ ).....	44
Figure 3-8 Contact angles and ellipsometric thicknesses of M9:M9C mixed SAMs as a function of growth solution mole ratio of M9 to M9C.. S: static, A: advancing and R: receding contact angles. ....	45
Figure 3-9 Surface composition of mixed M9:M9C SAMs calculated from the observed contact angles, plotted as a function of growth solution composition. S: static, A: advancing and R: receding contact angles.....	46
Figure 3-10 AFM images M9:M9C (1:1) mixed SAMs on template stripped gold surface. (1.25x1.25 $\mu\text{m}^2$ ).....	47
Figure 3-11 Contact angles and ellipsometric thicknesses of M9:M1C mixed SAMs. S: static, A: advancing and R: receding contact angles. ....	48
Figure 3-12 Surface composition of mixed M9:M1C SAMs calculated from the observed contact angles, plotted as a function of growth solution composition. S: static, A: advancing and R: receding contact angles.....	49

Figure 3-13 AFM images M9:M1C (1:1) mixed SAMs on template stripped gold surface. (1.25x1.25 $\mu\text{m}^2$ ).....	49
Figure 3-14 Calculated surface composition of all mixed SAMs based on advancing contact angles, plotted as a function of growth solution composition.....	50
Figure 3-15 Control experiments of pure SAMs in ethanol solution. ....	52
Figure 3-16 Contact angle measurements and ellipsometric thickness of M1 films in M9C solution. S: static, A: advancing and R: receding contact angles.....	53
Figure 3-17 Surface coverage of M1 films in M9C solution experiment.....	54
Figure 3-18 Contact angle measurements and ellipsometric thickness of M9C films in M1 solution SAMs. S: static, A: advancing and R: receding contact angles. ....	55
Figure 3-19 Surface coverage of M9C films in M1 solution experiment.....	56
Figure 3-20 Contact angle measurements and ellipsometric thickness of M9 films in M1C solution SAMs. S: static, A: advancing and R: receding contact angles.....	57
Figure 3-21 Surface coverage of M9 films in M1C solution experiment.....	58
Figure 3-22 Contact angle measurements and ellipsometric thickness of M1C films in M9 solution SAMs. S: static, A: advancing and R: receding contact angles.....	59
Figure 3-23 A) Contact angle measurements of M1 films in M9C solution and B)Contact angle measurements of M9C films in M1 solution respectively. S: static, A: advancing and R: receding contact angles.....	60
Figure 3-24 A) Surface coverage of M1 films kept in M9C solution. B) Surface coverage of M9C films kept in M1 solution.....	61
Figure 3-25 Contact angle values of (A) M9 films kept in M1C solution and (B) M1C films kept in M9 solution.....	62
Figure 3-26 Survey scan of M1 film.....	63
Figure 3-27 Peak fitting process for A) M1, B) 1:1 mixture of M9C and M1, C) M9C obtained from using XPS Peak Fit software.....	64
Figure 0-1 Raw data of M1, 1:1-Mix, M9C samples. ....	77
Figure 0-2 Raw data of M1 films kept in M9C solution 1.d,2.d, 3.d samples.....	78

## LIST OF ABBREVIATIONS

**SAM** Self Assembled Monolayer

**CAs** Contact Angles

**TS** Template Stripped

**TE** Thermally Evaporated

**CT** Carboranethiol

**AFM** Atomic Force Microscopy

**STM** Scanning Tunneling Microscopy

**XPS** X-Ray Photoelectron Spectroscopy

**M1** m-Carborane-1-Thiol

**M9** m-Carborane-9-Thiol

**M1C** m-Carboxylated-1-Thiol

**M9C** m-Carboxylated-9-Thiol

**BE** Binding Energy



## CHAPTER 1

### INTRODUCTION

#### 1.1. Background

Organic thin films were first created and examined by Irving Langmuir on the water surface in the 1940s. This type of thin-films are called Langmuir films [1]. These films are composed of a hydrophilic group that interacts with water molecules on one side and a hydrophobic group that does not interact with water on the other side thus molecules are dispersed on the liquid surface. Such molecules containing two different groups are called ‘amphiphilic’ molecules. Then studies have started on the preparation of these type films on solid surfaces. A thin film layer was formed on a solid substrate by submerging the solid slab into a beaker filled with a Langmuir film. These studies were conducted by Katherine Blodgett and this type of films are named as Langmuir-Blodgett films [2]. Blackman and Dewar continued investigation of organic thin films, and focused mainly on macroscopic properties such as wetting properties [2-4]. The first illustration in **Figure 1.1** represents the formation of a Langmuir film on a liquid surface. In the second and third illustrations, the formation and arrangement of films on substrates immersed in a liquid are schematized. In the last two illustrations, the preparation methods of self-assembled monolayer (SAMs) films are schematized. Self-assembly is the most often used method in the preparation of thin films. SAMs are “ordered molecular assemblies that are formed spontaneously by the adsorption of a surfactant with a specific affinity of its head group to a substrate in an organic solvent or by sublimation of the molecular adlayer in a vacuum” [5]. Various SAMs have been prepared and examined carefully. For instance, organosilicons on oxidized surfaces ( $\text{SiO}_2$  on Si,  $\text{Al}_2\text{O}_3$  on Al, glass, etc.); alkanethiols

on Au, Ag, and Cu; alcohols and amines on Pt; dialkyl sulphides and dialkyl disulphides on Au; and carboxylic acids on Al<sub>2</sub>O<sub>3</sub> and Ag [6-11]. In 1983, Nuzzo and Allara discovered SAMs of thiols and disulphides on Au (111) that have been intensively studied since then because of their interfacial properties and potential applications in molecular technologies. SAMs of thiols on Au(111) have been used to study important fundamental phenomena and processes such as adhesion [12,13], bonding [7], surface wetting [14-19], friction and lubrication [20], biocompatibility [21,28], protein and cell adhesion [29-33], interfacial electron transfer [34-40], and catalysis[38,41,42].

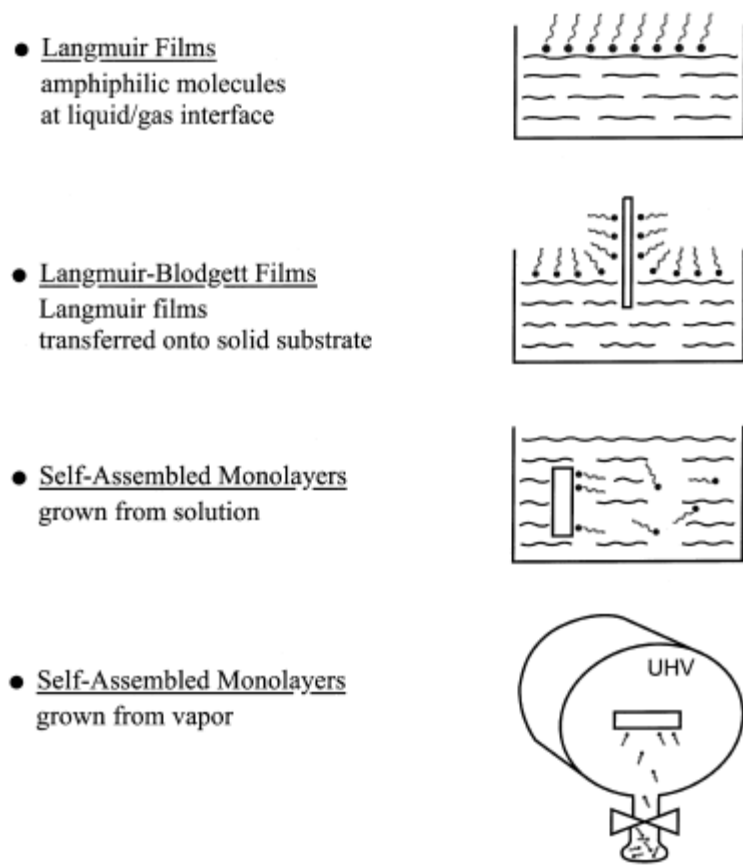


Figure 1-1 Overview of various preparation routes of organic thin films. Retrieved from ref [6].

## 1.2. Concept of Self-Assembly

SAMs are ordered molecular assemblies formed by the adsorption of an active surfactant on a solid surface. Self-assembled monolayers are formed of molecules that having three parts in their structure as shown in **Figure 1.2**.

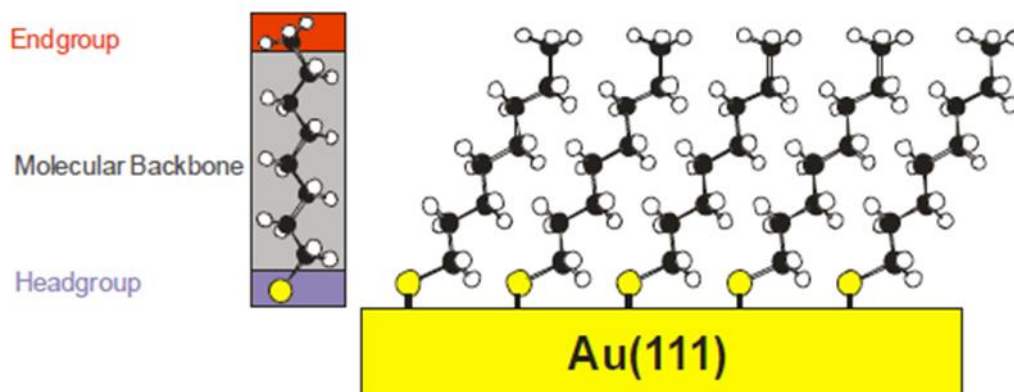


Figure 1-2 Schematic diagram shows the constituents of a SAM-molecule. Retrieved from ref [43]

### 1.2.1. Headgroup

Head group is the part of the molecule that binds to substrate via chemisorption. Highly strong molecular-substrate interactions enable the fixing of the headgroup to a specific site on the surface through a covalent bond. Substrate-headgroup interactions have selectivity when monolayers formed. For example, organosilanes bind to hydroxylated surfaces via a Si-O bond, thiols bind to gold via a S-Au bond, and carboxylic acids bind to silver via an ionic  $\text{COO}^- \text{Ag}^+$  bond. [44] Chemisorption of alkanethiols as well as of di-n-alkyl disulfides on gold gives indistinguishable monolayers [45], which apparently form the Au(I) thiolate ( $\text{RS}^-$ ) species. The mechanism in the formation of SAMs from disulfides is shown below which is an oxidative addition of the S-S bond to the gold surface.



The mechanism in the formation of SAMs from thiols is shown in below which can be considered as an oxidative addition of S-H bond to the gold surface, followed by a reductive elimination of the hydrogen.



Many theoretical calculations were also performed for the alkanethiol-gold bonding. Initially it was found that for adsorption of thiols on Au(111), 3-fold hollow site with hcp packing (**Figure 1.3**) is the most stable site with bond energy of about 100 KJ/mole [106]. Nevertheless, later theoretical studies have shown that the fcc sites are the most favorite adsorption sites for thiols [46]. In some other studies, the bridge sites were found to be the most stable and energetically preferred sites for the thiols [47, 48].

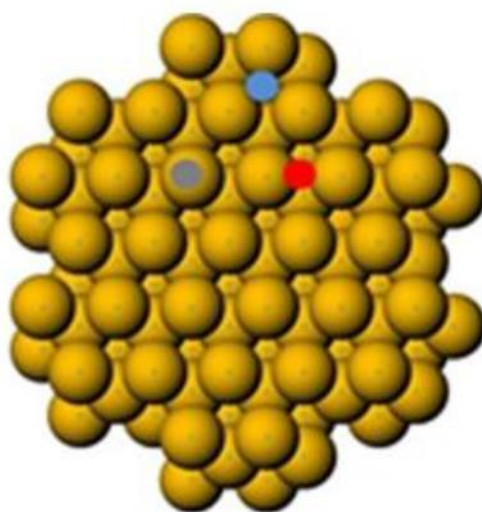


*Figure 1-3 The different absorption sites on Au (111). Grey dot represents “top” site, red dot indicates a bridge site and blue one corresponds to a hollow site (hcp or fcc).*

### 1.2.2. Molecular Backbone

A spacer or backbone group, consists of aliphatic or aromatic structure, is part of the molecule that links the headgroup to the end group. It has a significant role in

determining the order and structure in the SAMs. In SAMs, the formation of ordered and closely packed arrangement depends on the contribution of both intermolecular interactions, such as van der Waals, dipole, or  $\pi$ - $\pi$  interactions, and endgroup-endgroup interactions [49-52]. The strength of intermolecular interactions has been found to be governed by the backbone group and head group [53-54]. The conformation of the individual molecular backbones within the assembly and their packing, orientation, and ordering with respect to each other is determined by the relation between intermolecular interactions, inter-terminal group interactions, and the interaction with the surface. SAMs of sulfur-containing organic molecules with alkyl backbone have been examined extensively because of their well-ordered and close-packed surface structure, high stability, and the easy control of the surface properties. In recent years, oligophenylthiol SAMs which have an aromatic spacer group have drawn interest because of rigidity of their molecular backbone and strong  $\pi$ - $\pi$  interactions. These properties can provide higher stability for formed monolayer against thermally induced disorder which has been found to be an issue if alkyl derivatives were used [57,58]. In addition, aromatic thiols have been studied extensively due to their electronic properties and their capacity as building blocks for microelectronics [58-59]. There are some difficulties due to their solubility, which is lower than aliphatic SAMs, during preparation of aromatic thiols SAMs. This leads to low structural quality [60-63]. To overcome this problem and to enhance the flexibility of the spacer group of aromatic thiols aromatic-aliphatic mixed thiols were synthesized and the corresponding SAMs also have been investigated [64-67].

### **1.2.3. Terminal Group**

Terminal or end group is the end part of molecules forming the SAM that is responsible to functionalize the SAMs. Terminal group is responsible for successive adsorption [68,69] or chemical reaction on top of SAMs [70-73]. Self-assembled

monolayers on Au(111) ending with various functional groups such as fluorocarbons [74,75], OH, COOH [76-79], NH<sub>2</sub>, SH, CN [80], have been investigated with respect to their potential applications. A minor change in the terminal group can lead to major change in the physical and chemical properties of SAMs [81,82]. For example, SAMs functionalized with –CF<sub>3</sub> and –CH<sub>3</sub> groups gain hydrophobic, metallophobic and highly anti-adherent properties. On the other hand surfaces covered with COOH, -NH<sub>2</sub> or -OH functionalized SAMs were shown to be hydrophilic surfaces with good metal ion and protein binding properties [83,84]. A huge part of literature deals with binary mixed SAMs containing different terminal groups obtained by mixing differently terminated thiols in growth solution to vary surface properties such as wetting and reactivity [85,86]. Functionalized SAMs have a wide range of applications in surface science [87-92], surface engineering [17-18], sensor development [92], and preparation of nanoparticles [93,94] organic field-effect transistor [82,83].

### **1.3. Mechanism and Kinetics of SAM formation**

#### **1.3.1. SAM Formation**

There are two methods to adsorb thiol molecules onto Au (111) surface and these are gas-phase and solution-phase monolayer formation.

##### **1.3.1.1. Solution-phase monolayer formation**

Different surface analysis techniques were used to study the adsorption mechanism and kinetics of thiols on Au (111) in solution. These include ellipsometry [45], quartz crystal microbalance (QCM) measurements [46], surface plasmon resonance (SPR) spectroscopy, helium diffraction, scanning probe microscopies and X-ray photo

electron spectroscopy (XPS) [43,51]. Majority of these studies propose a two-step kinetic model for alkanethiol formation,

a) The first step takes place within the time scale of seconds to a few minutes, during which 80-90 % of the monolayer is formed.

b) The second step takes place with a time scale of minutes to hours during which monolayer undergoes orientational ordering leading to saturated phase or full coverage phase [49, 90, 91, 95].

Extensive research has shown that rate of monolayer formation increases with increasing concentration of thiol in the growth solution. When studying the kinetics of SAM formation from different solutions, the thiol concentration in the solution must be controlled carefully. For monolayer formation, the cleanliness of both the thiol source material and the solution is essential. Any kind of contamination will affect the adsorption mechanism. It has been reported that presence of contamination delays the monolayer formation [52].

### **1.3.1.2. Gas phase monolayer formation**

Gas phase monolayer formation is a more “straightforward” process than solution phase, because there are no solvent interactions which decrease the amount of contaminations. Moreover, the cleanliness of substrate can be controlled more precisely by using different in situ analysis techniques. During or after self-assembly process, diffraction and spectroscopic studies only provide spatially averaged information about the adsorption process. Hence there was a need for molecular level information about localized and heterogenous events. The reaction mechanism and kinetics of the self-assembly of thiols onto Au (111) from the vapor phase and from the solution (in-situ) have been studied well by using scanning tunneling microscopy (STM) and atomic force microscopy (AFM). As a result of these studies, a two-step mechanism for film formation have been found. In the first step, lying-down or striped

phase with molecular axis being parallel to the Au (111) surface forms as shown in **Figure 1.4** i-ii. The growth of the lying-down phase was found to follow a first-order Langmuir adsorption isotherm. In the second step, densely packed domains (standing-up phase) are formed after a two-dimensional phase transition which arise from several intermediate structures (**Figure 1.4** iii). Following this stage, molecules are oriented with their molecular axis almost perpendicular to the surface (**Figure 1.4** iv).

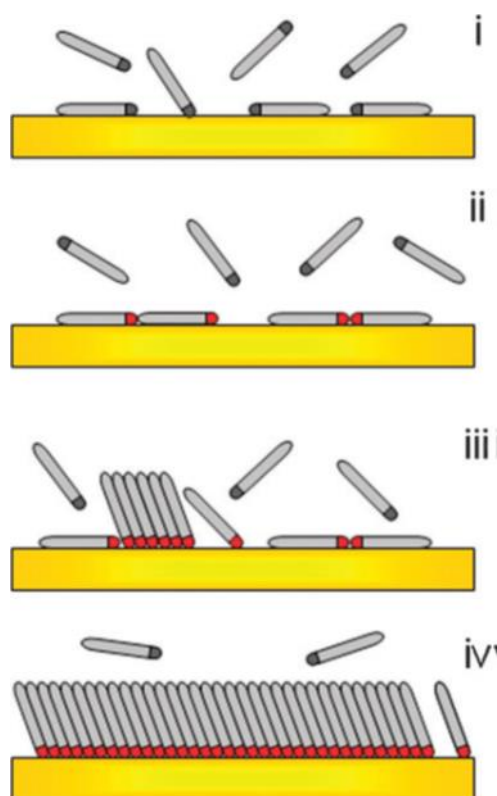


*Figure 1-4 Scheme of the different steps taking place during the self-assembly of alkanethiol on Au(111): (i) physisorption, (ii) lying down phase formation, (iii) nucleation of the standing up phase, (iv) completion of the standing up phase. Retrieved from ref [5]*

#### 1.4. Characterization of Thiol SAMs

There are several characterization techniques (AFM, XPS, STM, FTIR) to analyze thiol SAMs in terms of composition, topography and structure. Ellipsometry and

contact angle techniques can be used to characterize global properties like thickness and surface wettability. In our study we used contact angle, ellipsometry, AFM and XPS given in detail in the experimental section. As was mentioned in the beginning of introduction, extensive studies were performed by using alkanethiol SAMs on gold surface. Alkanethiol SAMs can be functionalized to obtain desired surface properties. For instance, the hydrophobic  $-\text{CH}_3$  end group increase the hydrophobicity of the surface but  $-\text{COOH}$  or  $-\text{OH}$  end groups increase the surface hydrophilicity. Contact angle,  $\theta$ , is a quantitative measure of the wetting of a solid surface by a droplet and gives valuable information about wetting properties of films and solid surface. Yosuhiko and his coworkers used contact angle measurements to characterize the  $\text{CF}_3(\text{CH}_2)_n\text{SH}$  and  $\text{CH}_3(\text{CH}_2)_n\text{SH}$  alkanethiols SAMs, where  $n=9-15$ , on gold surface. They found  $\text{CF}_3$  terminated alkanethiol to be more hydrophobic than  $\text{CH}_3$  terminated alkanethiol. Terminally fluorinated SAMs are highly oriented and densely packed like their hydrocarbon predecessors. Moreover, they also used ellipsometry to determine the thickness of films. Ellipsometry is based on the change in the polarization state of light as it is reflected obliquely from a thin film sample. Yoshurio and coworkers found that when number of carbon atoms in the backbone in  $-\text{CH}_3$  and  $-\text{CF}_3$  terminated alkanethiol SAMs was increased the thickness of film was also increasing as shown in **Figure 1.5** [82].

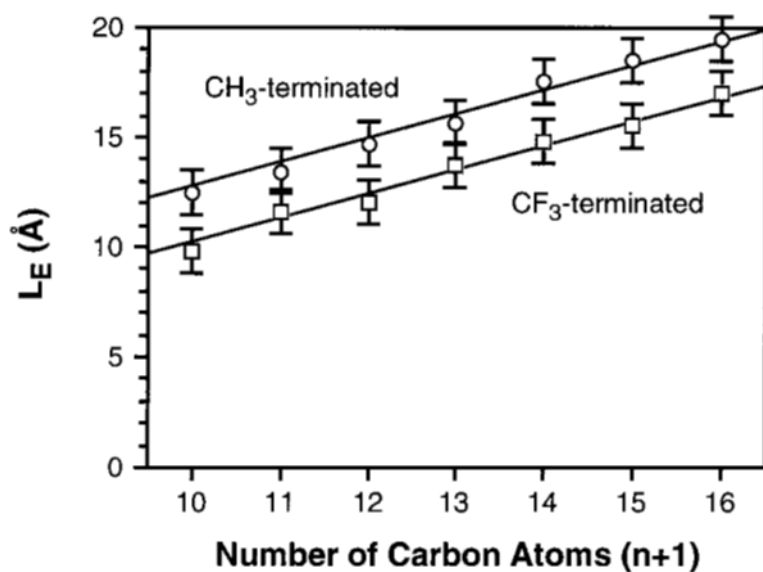


Figure 1-5 Ellipsometric thickness of SAMs. Line indicates calculated theoretical thickness. Retrived from ref [35]

Atomic Force Microscopy (AFM) is another technique to characterize thiol SAMs . AFM is based on measuring the interaction between a sharp tip and the sample surface. These interactions originate from various forces such as electrostatic, magnetic forces and van der Waals forces. Carla and coworkers studied different alkanethiol SAMs with different chain lengths (octadecanethiol, decanethiol and hexanethiol). Their aim was to investigate the behavior of these alkanethiol SAMs on Au surface in atomic level. In **Figure 1.6**, lattice structure of these SAMs can be seen. These images show that their lattice structure on Au is  $(\sqrt{3}\times\sqrt{3}) R30^\circ$ .

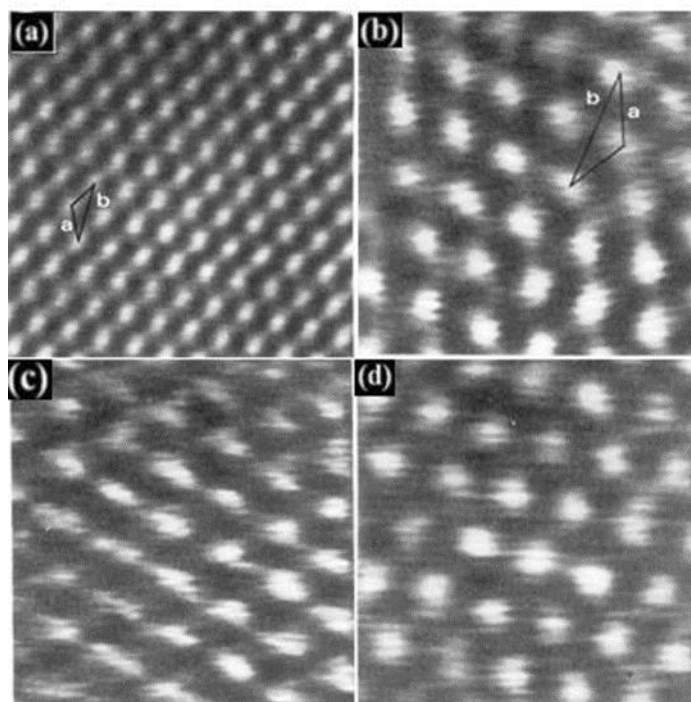


Figure 1-6 AFM image of bare Au(111) with hexagonal structure. b) AFM image Octadecanethiol on gold surface. Hexagonal structure of SAM is shown by vectors. c) AFM image of decanethiol. d) AFM image of hexanethiol. Retrieved from ref [96].

In addition, X-ray photoelectron spectroscopy (XPS) is also an important characterization technique for surface analysis. XPS is a surface analysis technique that uses the photoelectric effect to attain quantitative and qualitative information about the elemental composition and chemical state of the elements. Rieley and coworkers studied SAMs of 1,8-octanethiol and 1-octanethiol by using XPS. Their aim was to follow the alignment and photo-oxidation in these SAMs. They found that molecules in these SAMs were attached to the surface through a single Au-thiolate bond.

### 1.5. Carboranethiol (CT) SAMs

Thiolated dicarba-closo-dodecarborane have three isomers depending on position of carbons in the cluster. When the carbons are separated by one or two boron atoms the

isomers are named as Meta (m) and Para (p). The isomer with neighboring carbons in the cage is named as Ortho (o). Borane cage has pseudoaromaticity because of bond delocalization and electron deficiency in carborane. Carboranethiols (CTs) are chemically and thermally stable molecules to use as self-assemblies. CT isomerism can occur with substitution from both carbon and boron sites. They are suitable compounds for surface modification because of possibility of thiolation at different positions for the three isomers. By changing positions of carbon atoms in the cage, dipole moment and its direction can be controlled without changing the geometry of the molecule. For example, m-1-carboranethiol (M1) and m-9-carboranethiol (M9) are two thiolated derivatives of the parent meta isomer. For M1, thiol group is attached to carbon, while for M9, thiol group is attached to the boron. The structure of the above mentioned two compounds are presented in **Figure 1.7**.

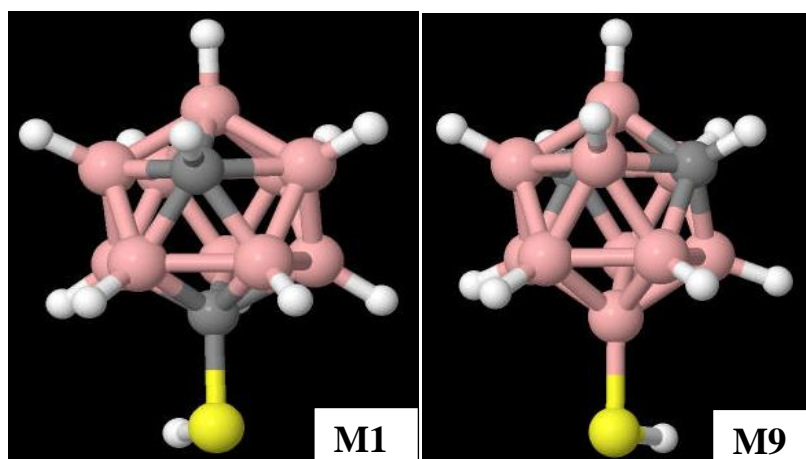


*Figure 1-7 Chemical structures of M1 and M9 carboranethiols. Grey: carbon, pink: boron, yellow: sulphur, white: hydrogen.*

Weiss and coworkers studied these two meta isomers, whose dipole moment vectors (pointing from negative pole to positive one) are shown in **Figure 1.8**. They prepared mixed SAMs of these isomers with different mixing ratios and studied their effect on the work function of gold surfaces [99].

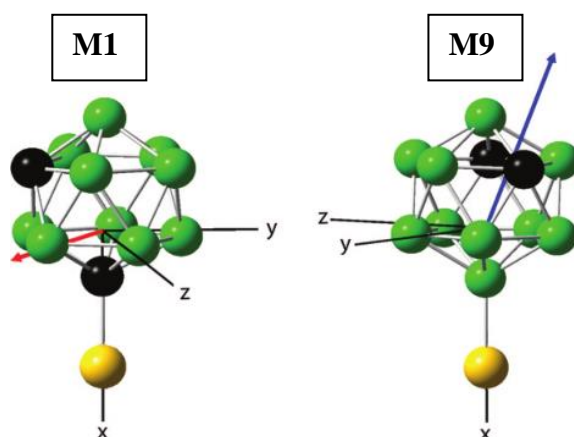


Figure 1-8 Dipole moment direction of M1 and M9. Retrieved from [99]

The positive end of the dipole moment vector is pointing between the carbon atoms for both cases. Dipole moments of M1 and M9 were calculated as 1.06 D and 4.08 D, respectively, by using DFT in a gas phase. The positive end of the dipole stabilizes the negative sulfur atom resulting in higher acidity of M1. The acidity of thiol on carborane isomers was reported be  $pK_a = 5.30$  and  $pK_a = 9.45$  for M1 and M9 respectively. SAMs of these isomers were characterized by using STM and CA measurements. STM results, **Figure 1.9**, show that M1 and M9 are topographically indistinguishable due to the similar apparent height. Fourier transformed STM image (inset in **Figure 1.9 A, B**) shows a nearest-neighbor spacing of  $7.2 \pm 0.4 \text{ \AA}$  for both M9 and M1 SAMs. Based on these results, two possible unit cell structures were proposed as  $(5 \times 5)$  and  $(\sqrt{19} \times \sqrt{19})R23.4^\circ$ .

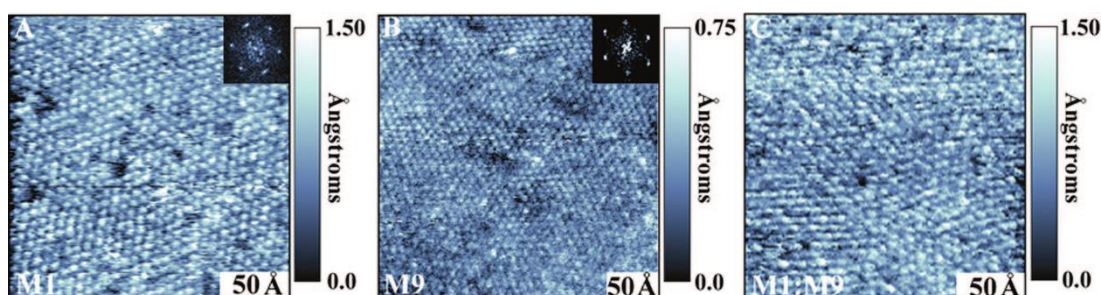
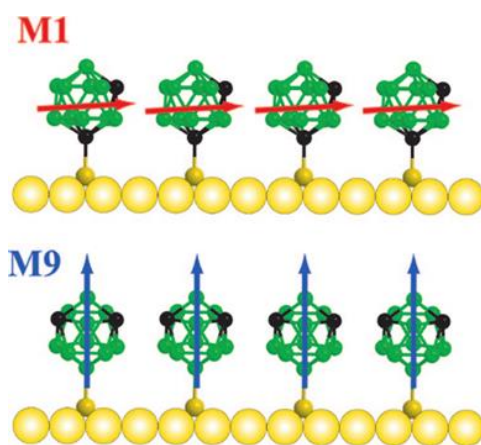


Figure 1-9 STM images of SAMs of A) M1. B) M9 and C) an adlayer prepared from a 1:1 solution on gold surface. Inset in A and B correspond to fourier transforms image A and B showing reciprocal lattice. Retrieved from ref [99].

Weiss and coworkers used Kelvin Probe Force Microscopy (KPFM) to measure the effect of M1 and M9 monolayers on the work function of gold surfaces arising from their different dipole orientations. The work function was decreased by  $90 \pm 20$  meV upon M1 adsorption whereas upon M9 adsorption it was decreased by  $480 \pm 20$  meV. The dipole moment of the M1 molecules are oriented nominally parallel to the surface, and are low in magnitude. On the other hand dipole moment vectors of M9 are oriented normal to the surface and have larger magnitude moment. A dipole more perpendicular to the surface will have a stronger influence on the work function, while one parallel to the surface will have a weaker influence. Therefore, M9 has higher impact on work function of gold surfaces. The results of CA measurements from Weiss group's study are given in **Table 1.1** All CT SAMs were found to be relatively more hydrophilic than the reference alkanethiolate (C12) SAM. M9 SAMs have larger dipole moment than M1 which makes M9 SAMs more hydrophilic. Even in the mixture of M1: M9 at 1:3 ratio, M1 was the dominant species on the surface. The authors explained such behavior with dipole moment direction of M1. Since M1 molecules have dipole moment nominally parallel to the surface, there is favorable head to tail dipole moment interaction between M1 molecules on the surface which stabilizes the SAM. (**Figure 1.10**)



*Figure 1-10 Head to tail dipole moment of M1 and perpendicular dipole of M9. Retrieved from ref [99]*



By performing a Fourier transform analysis of the STM images they determined the crystal structure of these SAMs to be a hexagonally close-packed arrangement with nearest-neighbor spacing of  $7.2 \pm 0.5 \text{ \AA}$  (shown in **Figure 1.12**). It was difficult to visualize single component SAMs of A' because of the strong hydrophilic COOH group that rotates almost freely around the fivefold symmetry axis of the p-carborane cage. Their XPS results, **Figure 1.13**, showed that most of the molecules of both derivatives adsorb as thiolates and just a small fraction of each adsorb as thiols. The advancing and receding contact angle values of A were  $87.5 (0.3)^\circ$  and  $76.8 (0.2)^\circ$ . The advancing and receding contact angle values of A' were  $30.0 (0.1)^\circ$  and  $24.8 (0.1)^\circ$ . A' has strong hydrophilicity because of COOH group which support the CA measurements results.

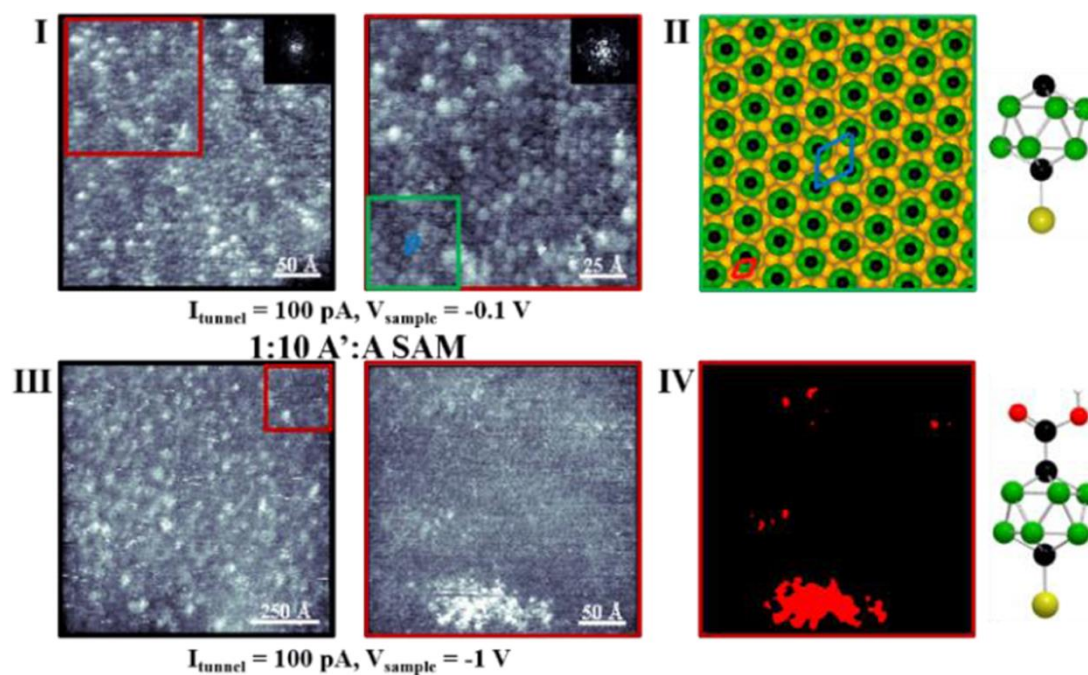


Figure 1-12 I) STM images of A. II) Observed lattice, blue lines indicates nearest neighbors. III) Mixed 1:10, A', A SAM. IV) Thresholding enables the isolation of A' regions that are highlighted in red. Retrieved from ref[102].

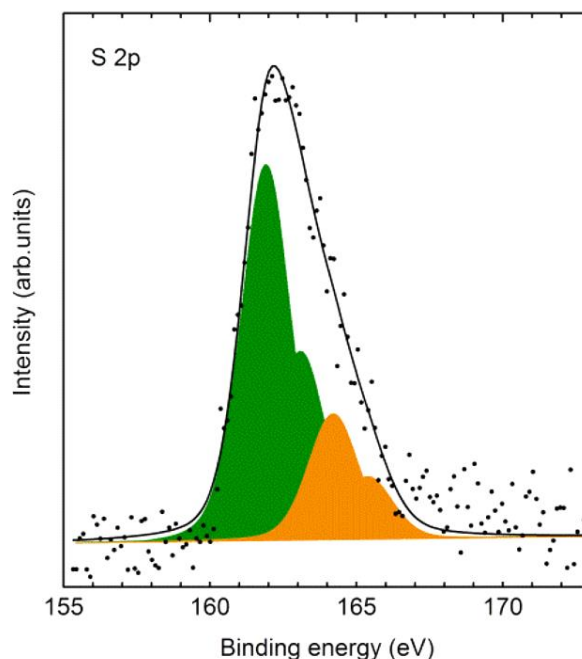


Figure 1-13 X-ray photoelectron spectrum of S 2p photoelectrons fit to indicate the contributions of both the thiolate (green) and the thiol (yellow) bound moieties of A' on gold surfaces. Retrieved from ref[102].

## 1.6. Motivation of Study

Weiss group showed that head to tail dipole-dipole interactions of M1 on the gold surface affects the film properties significantly [99]. Moreover, Base group showed that introducing carboxylic functional group to carborane isomers affects the film properties as well [102]. However, SAMs of carboxyl-functionalized meta carboranethiols in pure or mixed form have not been studied in the literature. In this study, considering the above mentioned groups' works, our motivation was to investigate the effect of meta isomers of carboxyl-functionalized CT SAMs on film properties. Since the magnitude and the direction of dipole moments of carboranes are distinct, mixed SAMs are expected to have different properties relative to their pure forms. To this end, we focused on two specific meta carboxyl-functionalized CTs: 1-COOH-7-SH-1,7-C<sub>2</sub>B<sub>10</sub>H<sub>10</sub> (M1C) and 1-COOH-9-SH-1,7-C<sub>2</sub>B<sub>10</sub>H<sub>10</sub> (M9C) (structures are shown in **Figure 1.14**). We prepared pure SAMs of these molecules in

addition to mixed SAMs of these with their unfunctionalized precursors (M1, M9). CA measurements were performed to investigate surface wettability. Ellipsometry was used for thickness determination. AFM was used to investigate the morphology and XPS was used to determine the electronic properties of these SAMs.

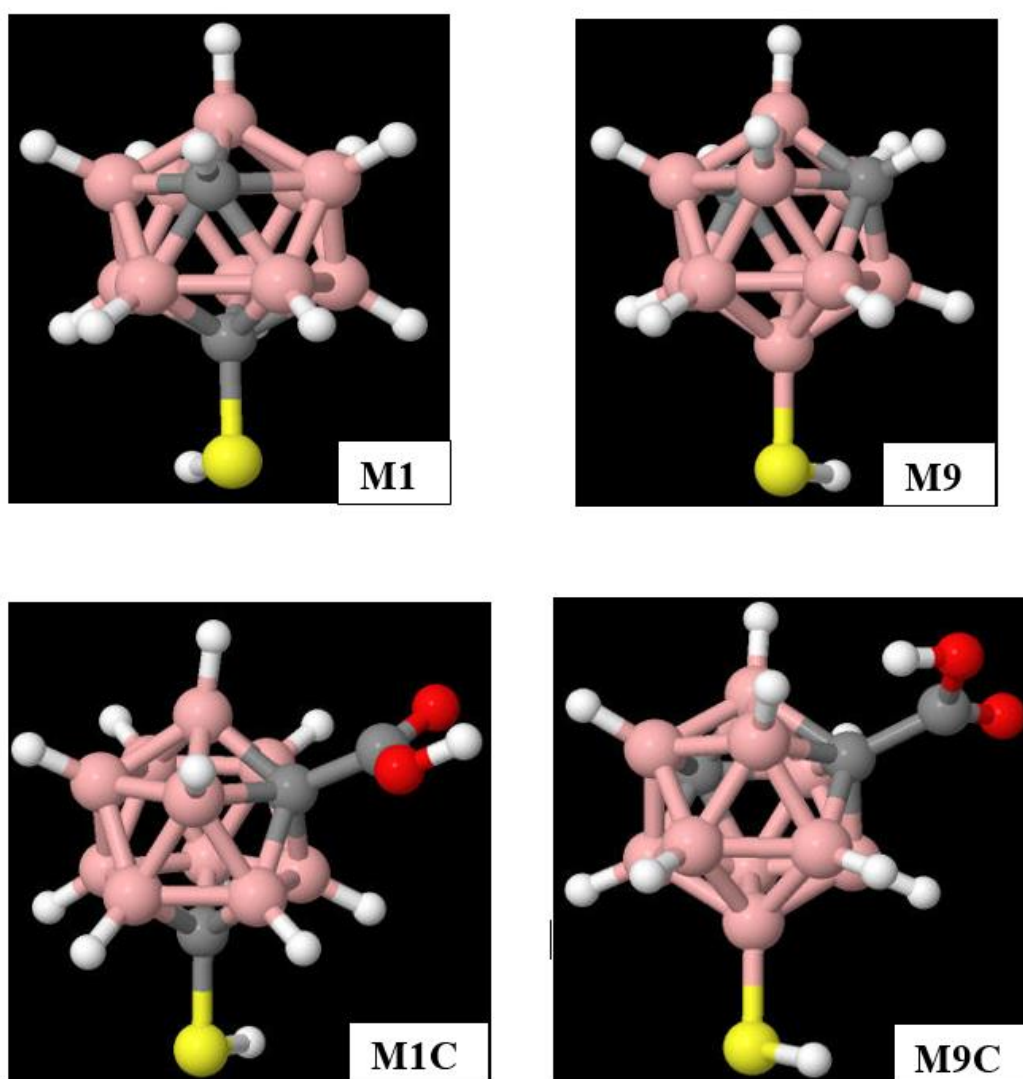


Figure 1-14 Four different carboranethiol molecules studied in this thesis. Grey:Carbon, Pink: Boron, Yellow: Sulfur, Red: Oxygen, White:Hydrogen.

## **CHAPTER 2**

### **EXPERIMENTAL**

In this part, firstly the theoretical background and working principles of characterization techniques used in this study will be introduced. Then, SAM preparation and characterization procedures will be discussed in detail.

#### **2.1. Characterization Techniques**

##### **2.1.1. Atomic Force Microscopy (AFM)**

The working principle of AFM is based on measuring the interaction between a sharp tip and sample surface. These interactions originate from various forces such as electrostatic, magnetic and van der Waals forces. There are three main components in an AFM which are cantilever with a sharp tip for probing, piezo-electric scanner for moving sample and split photodiode for measuring deflection of the cantilever. A laser beam is used to detect cantilever deflections towards or away from the surface. The laser is focused on the reflective back side of the cantilever. The reflected laser beam from cantilever is then focused on the center of a quadruple photodiode. Hence, laser will be deflected as cantilever deflects due to interaction with the surface and this deflection is measured by the photodiode. The working principle of AFM is depicted in **Figure 2.1**.

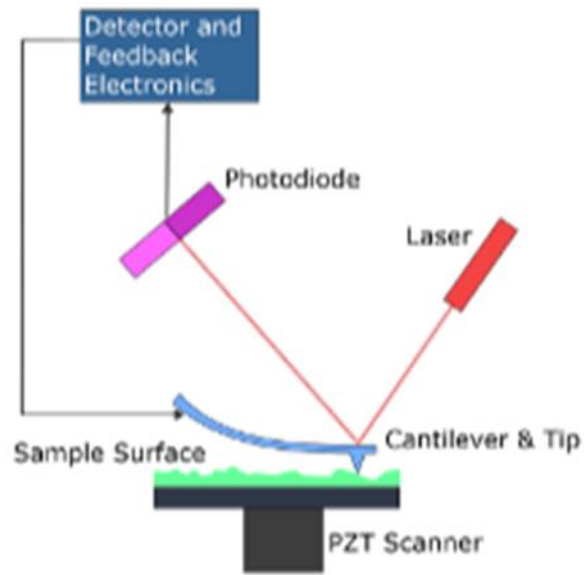


Figure 2-1 Schematic illustration of AFM working principle. Retrieved from [ref 99].

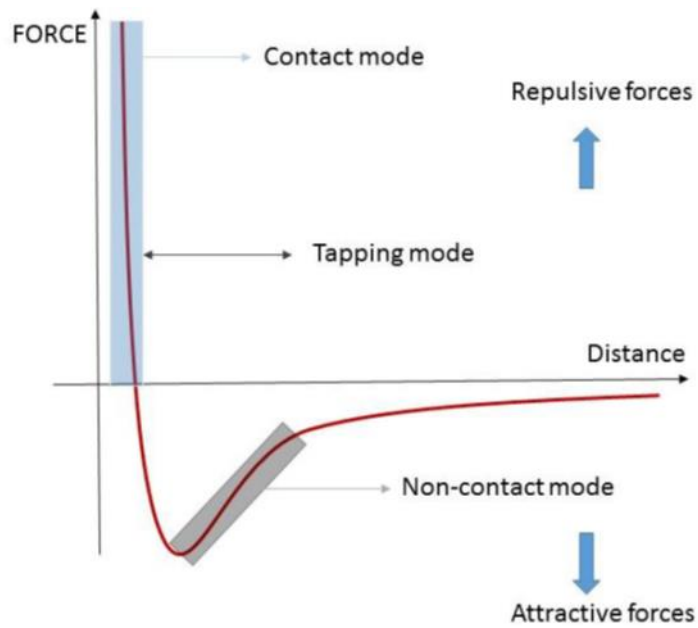


Figure 2-2 Illustrative force vs distance curve between the scanning tip and sample. Retrieved from ref [98].

In **Figure 2.2**, the force versus distance curve between a surface and the tip of a cantilever is shown. There is weak attraction between the tip and surface at larger distance. This attraction increases at specific distance when tip approaches to surface. AFM can be run in three different modes that are contact, non-contact and tapping mode by choosing a certain interaction region. In contact mode, cantilever is in physical contact with the surface thus strong repulsive force causes the cantilever to deflect as it passes over topographical features. Sample can be damaged because of the nature of the force. In non-contact mode, the cantilever oscillates just above the surface as it scans. Tip and surface are separated by a distance between 1 nm to 10 nm which leads to weak attractive forces between sample surface and tip. By using the feedback loop to correct for these amplitude deviations, one can generate an image of the surface topography. [95] In the tapping mode, the cantilever again oscillates just above the surface, but at a much higher amplitude of oscillation and in a way that it touches the surface intermittently. The bigger oscillation makes the deflection signal large enough for the control circuit, and thus an easier control for topography feedback. This mode is generally used for rough surfaces.

### **2.1.2. Spectroscopic Ellipsometry (SE)**

Spectroscopic ellipsometry (SE) is a very powerful optical technique for characterization of thin films. The working principle of SE is based on the change in the polarization state of linearly polarized light as it is reflected obliquely from a thin film sample. This change gives information about, sample roughness, thickness, surface composition, interface and optical properties like refractive index of thin films. General procedure for data collection and analysis in ellipsometry can be summarized in three parts. Firstly, a polarized light is generated and reflected whose polarization state changes due to reflection. Secondly, reflected light is monitored and analyzed in terms of the complex reflectance ratio ( $\rho$ ) which is a function of  $\psi$  and  $\Delta$  (which will be explained below in detail). Finally, desired properties and thickness are obtained through modelling and parameter fitting to raw data. The incident and the reflected

beam span the plane of incidence. Light which is polarized parallel to this plane is named p-polarized, if the polarization is perpendicular to this plane it is referred as s-polarized. These parts are presented in **Figure 2.3**. Spectroscopic ellipsometry measures  $\psi$  and  $\Delta$ .  $\psi$  is the ratio of the amplitude of the p polarized component of the light to s polarized component. Its formula is shown in equation 1 where  $r_p$  and  $r_s$  are the Fresnel reflection coefficients.

$$\tan(\psi) = \frac{|r_p|}{|r_s|} \quad (2.1)$$

$\Delta$  is the phase difference between the p and s polarized light. Its formula is given in equation 2, where  $\delta_p$  is the phase change in p polarized light and  $\delta_s$  is the phase change in s polarized component upon reflection from sample surface.

$$\Delta = \delta_p - \delta_s \quad (2.2)$$

Ellipsometry allows for the determination of the complex reflectance ratio  $\rho$  of a surface.

$$\rho = \frac{R_p}{R_s} = \tan(\psi) e^{i\Delta} \quad (2.3)$$

$$\rho = f(N_0, N_1, N_2, \lambda, d_1, \theta_0),$$

$R_p$  and  $R_s$  are the coefficients that are analogues to  $r_p$  and  $r_s$  that are relevant for a single interface system. Complex reflectance ratio,  $\rho$ , is based on the incidence angle ( $\theta_0$ ) and the wavelength ( $\lambda$ ) of the light and thickness of the film ( $d_1$ ) and complex refractive indices ( $N=n+ik$ ).  $N_0$ ,  $N_1$  and  $N_2$  are the refractive indices for the ambient, film and the substrate, respectively. It should be noted that  $N_j$ , which is also named as

optical constant, further depends on ( $\lambda$ ) and thicknesses ( $d_j$ ) of all the layers (labeled by  $j$ ) in the sample.

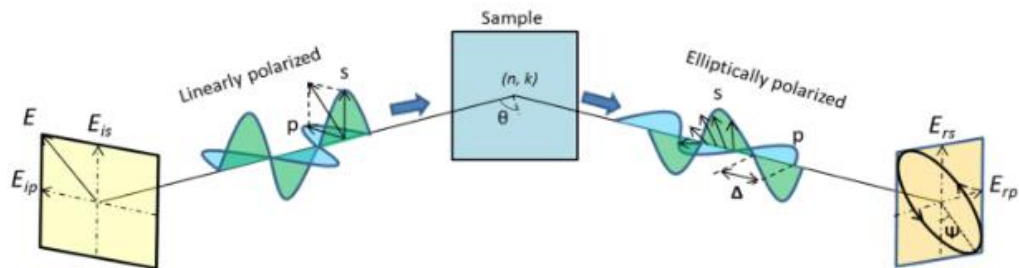


Figure 2-3 The working principle of spectroscopic ellipsometry. Retrieved from ref [96].

$\psi$  and  $\Delta$  are measured as a function of wavelength ( $\lambda$ ) at fixed incidence angle ( $\phi_0$ ). Therefore, the thickness and the refractive indices of all the layers could be determined by fitting the experimentally measured  $\psi$  vs.  $\lambda$  and/or  $\Delta$  vs.  $\lambda$  curves to a function (based on Fresnel equations) which parametrically depends on  $d_j$  and  $N_j$ . There are many different dielectric function models to acquire  $N_j$  as a function of wavelength. While Cauchy and Sellmeier models are used for semi-transparent and transparent films, Drude-Lorentz and Lorentz models can be used for opaque films.

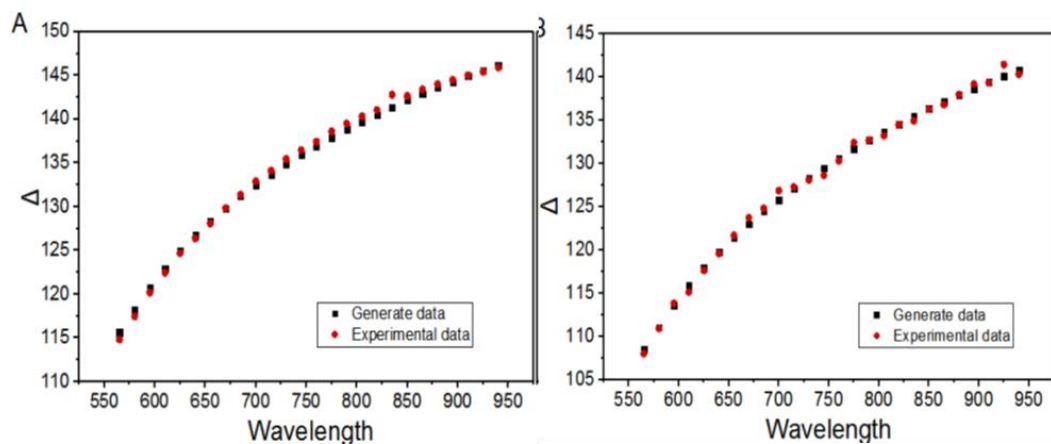


Figure 2-4 Experimentally measured data fitted with models A) Fitted template stripped gold film by using Drude Lorentz dielectric function and gold/air two phase model. B) Fitted carboranethiol film by using the reference gold parameters, Cauchy dielectric function for SAM and gold/Sam/air three phase model. Retrieved from ref [98]

We used three phase model because our samples consist of three layers: gold-SAM-air. In our experiments, Cauchy model was used to model dielectric properties of SAMs, by using the measured refractive index value of CTs for visible light. Firstly, measurement of bare gold film is made and modelled as two-phase model as gold-air. All the parameters for gold film are determined and used as reference which is shown in **Figure 2.4A**. Secondly, SAM is grown on the measured gold film which is mentioned earlier so the resulting sample is modelled by using the three phase model which is shown in **Figure 2.4B**. The thickness of SAM is acquired by fitting with an MSE value of 0.08-0.5, because reference parameters for gold is known.

### 2.1.3. Contact Angle

Contact angle,  $\theta$ , is a quantitative measure of the wetting of a solid surface by a liquid (droplet) and gives valuable information about wetting properties of films and solid surfaces. Young's formula presented in equation 2.4 can be used to determine the contact angles and is based on the interfacial tensions of air, liquid and solid.

$$\gamma_{lv} \cos \theta_Y = \gamma_{sv} - \gamma_{sl} \quad (2.4)$$

In this equation  $\gamma_{lv}$ ,  $\gamma_{sv}$ , and  $\gamma_{sl}$  represent the liquid-vapor, solid-vapor, and solid-liquid interfacial tensions, respectively, and  $\theta_Y$  is Young's contact angle.

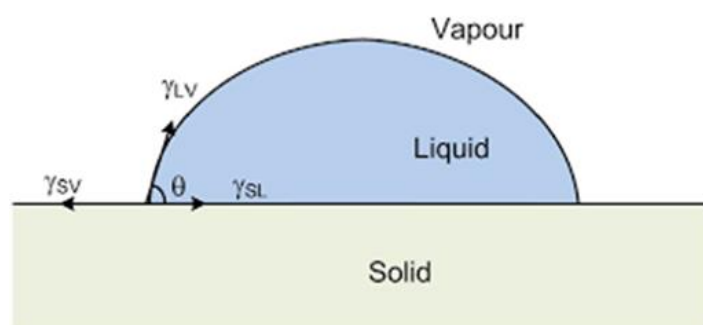


Figure 2-5 Young's construction of the force balance at a three phase contact line between a droplet, its vapor, and a solid surface. Retrieved from ref [5].

Young's equation is valid for an ideal surface. Since real surfaces are not ideal several models were developed to describe the contact angles on real surfaces. Two such models are the Wenzel model and the Cassie-Baxter model. Real surfaces can have chemical heterogeneity and surface roughness. While Wenzel model considers rough surfaces with chemical homogeneity [1]. Cassie's model considers flat surface with chemical heterogeneity [2, 6]. Wenzel equation is (2.5) as follows:

$$\cos \theta^* = r \cos \theta_Y \quad (2.5)$$

where  $r$  is the roughness factor (the ratio of total surface area to the projected area in the horizontal plane),  $\theta$  is the contact angle measured on the flat surface and  $\theta^*$  is the observed contact angle.

This model proposes that observed contact angle on hydrophilic surfaces ( $\theta < 90^\circ$ ) will decrease while on hydrophobic surface ( $\theta > 90^\circ$ ) will increase as roughness of surface increases. Cassie's equation which is generally used for mixed SAM surfaces, is (2.6) as follows:

$$\cos \theta^* = \sigma_1 \cos \theta_1 + \sigma_2 \cos \theta_2 \quad (2.6)$$

Where  $\theta_1$  and  $\theta_2$  are the contact angles for the two components respectively and  $\sigma_1$  and  $\sigma_2$  ( $\sigma_1 + \sigma_2 = 1$ ) are the fractional coverage of the two components. In this model the components of film are assumed to behave independently, and surface composition of the film ( $\sigma_1$  and  $\sigma_2$ ) can be determined if  $\theta_1$ ,  $\theta_2$ , and  $\theta^*$  are known. Though this assumption may not be valid for many films, the model can still be used for approximate/qualitative results and for comparison purposes. In this study, Cassie's model was used to determine the composition of mixed CT SAMs that were examined.

### **2.1.3.1. Static contact angle**

Static contact angles are measured when the droplet is standing on the surface and the three-phase boundary is not moving. Static contact angle measurements are done for

obtaining information about the interaction of solid and the probe liquid on smooth and homogenous surfaces. Moreover, wetting properties of surface can be determined by these measurements (the hydrophobicity/hydrophilicity). In **Figure 2.6**, a representative static contact angle measurement result of 1-Octadecanethiol SAM on gold surface is shown where the angle was measured to be  $110.05^\circ \pm 0.02$ .

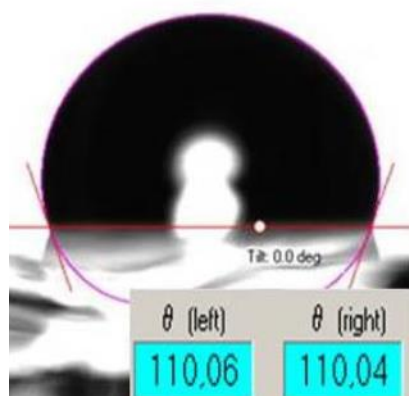


*Figure 2-6 Static contact angle of 1-Octadecanethiol SAM on thermally evaporated gold on mica.*

### **2.1.3.2. Dynamic contact angle**

In practice, the observed contact angles are not exactly equal to Young's contact angle because there are many meta stable states of a droplet on a solid. Thus, only the measurement of static angle is not enough to characterize the surface wetting properties. One way to obtain more detailed surface wetting properties is measuring dynamic contact angles. Dynamic contact angles are measured when three-phase contact line is in actual motion. Particularly, the contact angles that form when expanding (shrinking) the liquid are studied via increasing (decreasing) the volume of liquid which causes the edges of the droplet to advance (recede). Advancing angle is the maximum value that the angle reaches, receding angle is the minimum value that the angle reaches. In **Figure 2.7**, the illustration of advancing and receding angles is presented. Dynamic contact angle measurements can be done at different rates of

expansion (contraction) of the liquid droplet. The difference between receding and advancing contact angles is named as hysteresis and its formula is given in equation 2.7.

$$H = \theta_A - \theta_R \quad (2.7)$$

Where  $\theta_A$ ,  $\theta_R$  are advancing and receding angles respectively. From hysteresis values, surface heterogeneity and roughness can be interpreted.

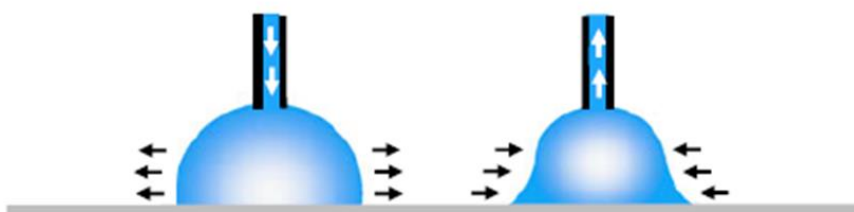


Figure 2-7 Illustration of advancing and receding angle. Retrieved from ref [99]

#### 2.1.4. X-Ray photo-electron spectroscopy (XPS)

XPS is a surface analysis technique that uses the photoelectric effect to attain quantitative and qualitative information about the elemental composition and chemical state of the elements. XPS probes surfaces up to a depth of 2-5 nm for characterization due to the mean free path of electrons in the solid state [101]. The energy of the incident radiation used in XPS is usually more than 1000 eV. Most extensively used sources to obtain X-rays in XPS are Aluminum  $K\alpha$  and Magnesium  $K\alpha$  (Mg) lines with the energies of 1486.6 eV and 1253.6 eV respectively [102]. Under UHV, when a sample is bombarded with X-rays of a characteristics energy, electrons from the core levels of the element are ejected. **In Figure 2.8**, these levels are presented. By using proper electron energy analyzer, the kinetic energy ( $K_E$ ) of the emitted photoelectrons and then the binding energy of the electrons ( $E_B$ ) can be measured. In the context of XPS “binding energy” refers to the energy required to remove an electron from an atom. Binding energy depends on the type of atom from

which the electron is emitted, the orbital from which the electron is ejected, the oxidation state of the atom and the chemical environment of the atom. According to Koopman's approximation, binding energy can be calculated by using equation 2.8 [100].

$$E_B = h\nu - E_{\text{Kin}} - \phi \quad (2.8)$$

Where  $\phi$  is the work function of the spectrometer,  $E_{\text{Kin}}$  is the kinetic energy of emitted photoelectron,  $E_B$  is the binding energy of a core level in the sample and finally  $h\nu$  is the energy of the exciting X-ray radiation. The XPS spectrum can be converted to a plot of photoelectron intensity, number of electrons per unit time, as a function of binding energy with known values of  $\phi$  and  $h\nu$ . The peaks appear in an XPS spectrum at distinct values of  $E_B$  hence the spectrum provides a "fingerprint" of the elements in the material and their chemical environment [100]. XPS is as a quantitative chemical spectroscopy technique since the area of a photoemission peak is proportional to the number of emitters in the analysis volume. In this study, XPS was used to identify the elemental composition of SAMs in replacement experiments which will be explained in results and discussion part elaborately.

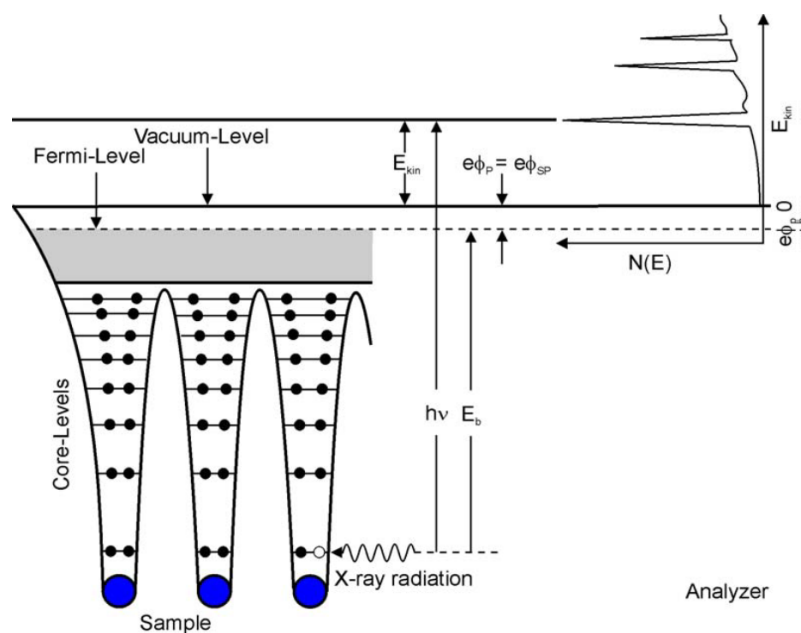


Figure 2-8 Schematic diagram of photoelectron spectroscopy. Retrieved from ref [101].

## 2.2. Specific Experimental Procedure

In this part, details of the gold substrate and SAM preparation procedures and working parameters of instruments that were used in this study will be described. In **Figure 2.9** general experimental procedure scheme is shown. Each part of the scheme will be explained in detail in the following parts.

### 2.2.1. Materials

The chemicals, o-carboran-1-thiol (98%), m-carborane-1-thiol (96%) and m-carborane-9-thiol (97%) were purchased from Katchem Ltd (Czech Republic) and Ethanol (99.8%) and Acetone (99.5%) were purchased from Sigma-Aldrich. All chemicals were used without purification. Carboxylic acid functionalized m-carborane-9-thiol (M9C) and m-carborane-1-thiol (M1C) were provided by Dr. Tomas Base at the Institute of Inorganic Chemistry, the Czech Academy of Sciences. 99.99% pure certified gold was purchased from Istanbul Gold Refinery. 99.99 % pure silver

were purchased from KJL company. Ruby muscovite mica, used as substrate for gold and silver film preparation, was purchased from S&J trading Inc (USA). Norland optical adhesive 61 (USA, purchased from Optomek Ltd Turkey distributor) and SU-8 2000 from Microchem (USA) were used for template stripped gold and silver preparation.

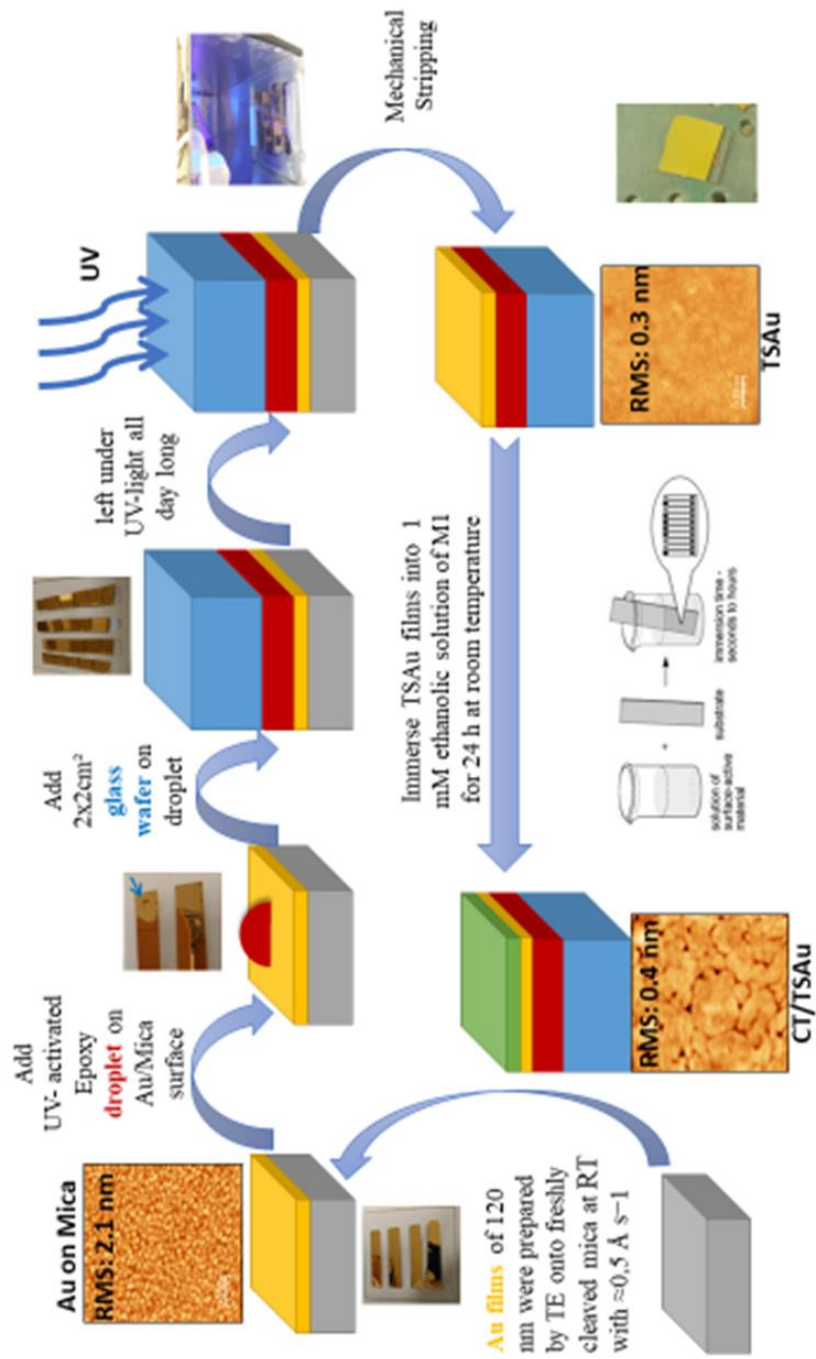


Figure 2-9 Scheme of general experimental procedure.

### 2.2.2. SAM preparation

Freshly prepared template stripped gold films rinsed with ethanol and dried in N<sub>2</sub> stream. These gold films were immersed into 1mM ethanolic growth solution of the investigated carboranethiol isomer (or isomers in case of mixed SAMs) for 24 h at room temperature for SAM preparation. Growth solutions were prepared freshly from 5 mM stock solutions. Stock solutions older than six months were not used to prevent degradation of CT molecules in ethanol due to the ethyl ester formation in ethanol solution. Slides were taken off from solution, rinsed with ethanol and dried with N<sub>2</sub> stream for characterization. For each set of conditions, at least 3 parallel SAM samples were prepared to ensure/confirm the reproducibility of the results. Same procedures were followed for SAMs on template stripped silver surfaces.

### 2.2.3. Template stripped (TS) gold and silver film preparation

Flat gold surfaces were important for our work since we want to study morphological properties of mixed carboxylated CT and mixed SAMs. For this purpose, template stripping technique was used which was optimized as a standard procedure in our research group in previous studies [98]. Here we will summarize the basic steps of this procedure and the details can be found in reference 98. To prepare template stripped (TS) gold films firstly, thermally evaporated, TE, gold films were prepared on freshly cleaved mica surfaces. The thermal evaporator in GÜNAM laboratories in the Chemistry Department was used to prepare Au films on freshly cleaved mica wafers with 15x15 cm<sup>2</sup> size. For reaching a deposition rate of  $\approx 0.4 \text{ \AA s}^{-1}$ , tungsten boat loaded with gold was heated to 1250 °C. During deposition, the thickness of Au films was approximately 120 nm which was monitored by a quartz crystal oscillator. Deposition was carried in a deposition chamber with base pressure of  $1 \times 10^{-6}$  mbar, pumped by an oil-free pump, at room temperature. Such TE gold films have high roughness values (about 1.5 nm), as measured by AFM and shown in **Figure 2.10**, and are not appropriate for our studies as mentioned above. Hence, in order to obtain atomically

smooth TS gold films were prepared by using freshly prepared TE gold films as will be described below.

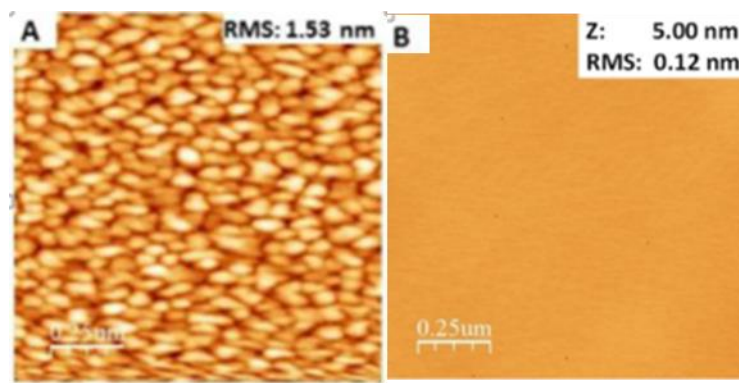


Figure 2-10 A) AFM images of thermally evaporated gold on mica. B) AFM image of TS gold film. Retrieved from ref [98]

Glass slides were cut into 1 cm x 1cm pieces and cleaned in piranha solution followed by rinsing with de-ionized water and absolute ethanol. About 2 mg droplets of epoxy resin SU-8 photoresist were dripped on TE gold films [step (2) in Figure 2.11] and cleaned glass pieces were placed on each droplet of epoxy [step (3) in Figure 2.11] thus forming a mica/gold/epoxy/glass sandwich. Glass pieces were, then, gently pressed (in a controlled way by using standard weights or clamps to have adequate pressure which is crucial) for assuring uniform spreading of the epoxy. Next the sandwiches were kept under UV light for a day (24 hour) [step (4) in Figure 2.11]. In the final step, the mica layer could easily be cleaved by tweezers so the atomically smooth mica/gold interface was exposed and TS gold films were obtained [step (5) in Figure 2.11]. The electrical conductivity of freshly prepared TS gold (TSAu) film surfaces was controlled at different points on the films by using a voltammeter to confirm no mica sheets/pieces were left on the gold surface. Using this procedure TSAu films could be prepared by 80% efficiency. That is, out of 10 sandwiches prepared 8 yield good TSAu films with average roughness of about 1 Å. A representative AFM image of TSAu films, with roughness of  $0.12 \pm 0.05$  nm., is shown in **Figure 2.10**.

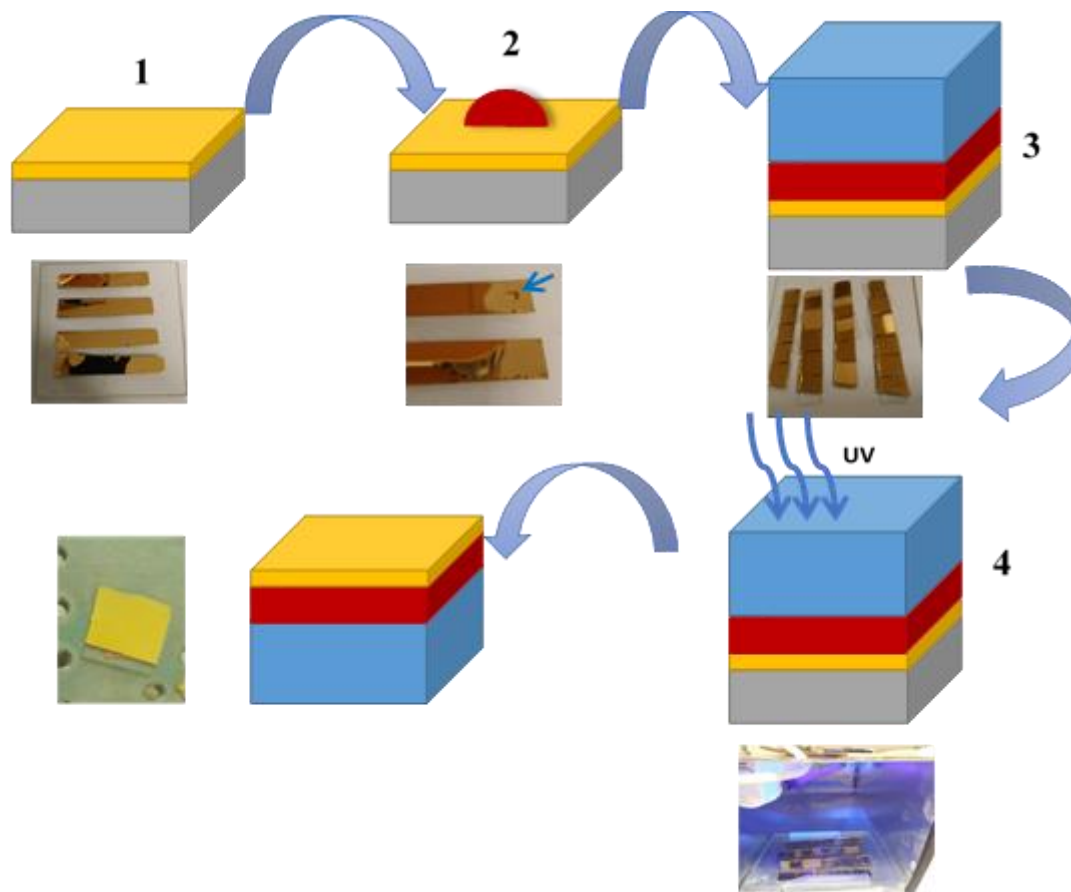


Figure 2-11 Illustration of template stripped gold surface preparation procedure.

#### 2.2.4. Contact angle

Contact angle measurements were performed by using an Attension Theta Lite optical tensiometer. For static contact angle measurements, a 3  $\mu\text{l}$  drop of de-ionized water was used. Dynamic sessile drop method was used to obtain dynamic contact angle of water. In this method, a sample is placed near the tip of a needle attached to a micro-syringe. A drop of de-ionized water (about 3  $\mu\text{l}$ ) is, then, formed on the surface of the sample and the needle is positioned in the center of the drop carefully without

changing droplet's shape. By increasing the volume of the droplet on the surface to a size of 5  $\mu\text{l}$  at constant rate the advancing contact angles were measured. By decreasing the volume of drop on the surface to a size 3  $\mu\text{l}$  the receding contact angles were measured. One of the important parameters in these measurements is the speed of expansion and contraction of the droplet and was kept constant and equal during advancing and receding measurements. The images of expanding (shrinking) drop were recorded at 18 frames/second for three seconds. The images were then analyzed by an automated image analysis software which gives right and left contact angles from the shape of the drop with an accuracy of  $\pm 0.1^\circ$ . At least three parallel samples were prepared for each SAM composition investigated and on each sample, measurements were performed on three different positions on the surface. In result and discussion part, each data point reported in the contact angle graphs corresponds to the average of such measurements with the associated errors.

#### **2.2.5. Spectroscopic ellipsometry**

Ellipsometric measurements were made by using a PhE-102 Variable Angle Spectroscopic Ellipsometer (VASE) equipped with a 75W Xe lamp working in the range of 250 nm- 1100 nm at an incident angle of  $65^\circ$ . The spot size was 1.5 mm. Before SAM preparation, reference ellipsometry data were recorded for the clean TSAu substrates. After the SAM formation ellipsometry data were recorded again after proper cleaning step (rinsing with absolute ethanol and drying with  $\text{N}_2$  stream). The film was accepted to be isotropic and assigned a scalar refractive index value of  $1.57 + 0i$  and film thickness calculations were carried on a three-phase ambient-film-gold model as described in section 2.1.2. At least three parallel samples were prepared for each SAM composition investigated and, on each sample, measurements were carried out on three different positions on the surface. In result and discussion part, each data point reported in the ellipsometric thickness graphs corresponds to the average of such measurements with the associated errors.

### **2.2.6. Atomic force microscopy**

AFM measurements were performed by using either Ambient AFM/MFM (Nanomagnetics instruments, Ankara). The measurements were carried out in air at room temperature by use of a Silicon cantilever, rectangular with a length of 225  $\mu\text{m}$  and force constant of 48 N/m. All images, 2.5x2.5  $\mu\text{m}^2$ , were acquired at constant amplitude in tapping mode. Contact mode measurements were performed by use of a soft silicon cantilever (rectangular with a length of 350  $\mu\text{m}$  long and width of 35  $\mu\text{m}$ ) with a force constant of 0.03 N/m. All image analysis processes were performed by using Gwyddion software.

### **2.2.7. X-Ray Photoelectron Spectroscopy**

In this study, XPS measurements were performed at UNAM in Ankara. The ex situ X-ray photoelectron spectra were measured by using a Thermo Scientific K-Alpha (Thermo Fisher) spectrometer, equipped with a monochromatic Al source with 400  $\mu\text{m}$  spot size and a hemispherical electron analyzer fixed at 45° with respect to the surface normal. The X-ray spectrometer was calibrated with the Au 4f<sub>7/2</sub> peak at 84.0 eV. The photoelectrons of Au 4f, C 1s, B 1s, O 1s, and S 2p were measured at room temperature. The high-resolution spectra of S and B were recorded with 30 scans and the operating pressure of the analyzer chamber was about  $2 \times 10^{-9}$  mbar. XPS Peak analysis software was used for curve fitting with the Gaussian: Lorentzian ratio being constant at 70:30%. [100] SAM samples were freshly prepared before XPS measurements: After removal from the growth solution, the samples were rinsed with ethanol, dried with N<sub>2</sub> and immediately placed in the XPS chamber to minimize contamination and oxidation.

## CHAPTER 3

### RESULTS AND DISCUSSION

#### 3.1. Pure carboranethiol self-assembled monolayers

In **Figure 3.1**, contact angles and ellipsometric thickness values for both unfunctionalized and carboxyl functionalized CT SAMs are presented. In **Table 3.1** their contact angles and hysteresis values are tabulated along with the reference values from one past study in the literature [99]. When compared with the literature results, the contact angle values we obtained for the unfunctionalized CT SAMs are significantly higher with larger standard deviations. Nevertheless, this much difference is acceptable when the standard deviations of our results are considered. As expected carboxyl functionalized SAMs have much lower contact angles than unfunctionalized ones due to the interaction of carboxyl groups with water. Interestingly, however, the contact angles of M9C is significantly lower than M1C. In **Table 3.1**, different contact angle values are shown from literature.

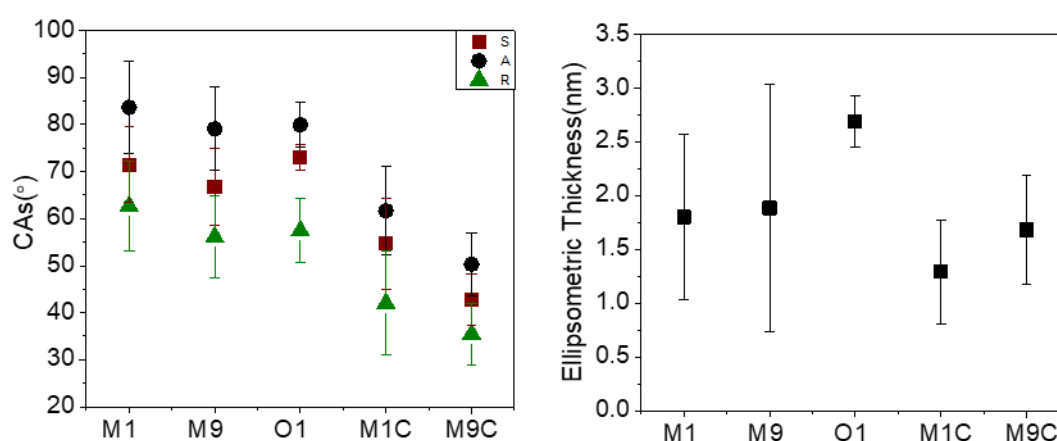


Figure 3-1 Contact angles and ellipsometric thickness for pure and carboxylated carboranethiols. S: static, A: advancing and R: receding contact angles.

Table 3.1 Contact angles of carboxylated and pure carboranethiol SAMs. Literature values from reference [99] are given in parenthesis.

	<i>Static</i>	<i>Advancing</i>	<i>Receding</i>	<i>Hysteresis</i>
<b>M1</b>	71.5±8.0	83.7±9.7	62.7±9.6	21.0
	(85.4±1.8*)	(90.1±1.6*)	(70.4±3.9*)	(19.7*)
	(85.8±1.1***)	(82±2**)	(71±1**)	(11.1**)
<b>M9</b>	66.8±8.2	79.1±8.9	56.1±8.7	23.0
	(74.4±1.4*)	(86.8±4.7*)	(54.3±3.4*)	(32.5*)
	(85.5±0.8***)	(72 ±4**)	(52±1**)	(20.3**)
<b>O1</b>	72.9±2.7	79.9±4.8	57.5±6.7	22.4
	(71.2±0.7*)	(78.0±1.8*)	(52.8±4.9*)	(25.2*)
<b>M1C</b>	54.7±9.7	61.7±9.4	42.0±11.0	19.7
<b>M9C</b>	42.7±5.5	50.3±6.6	35.5±6.5	14.8

\* Results from previous studies of our group, \*\* From Weiss Group (1), \*\*\* From Weiss Group (2)

### 3.2. Mixed carboranethiol self-assembled monolayers

In this part of the thesis studies mixed CT SAMs were examined. Specifically, M1:M1C, M9:M9C, M1:M9C and M9:M1C mixed SAMs were prepared and characterized. The thickness of all mixed SAMs were nearly equal and about 1.5 nm, regardless of the surface composition, in agreement with the theoretical height of the CT molecules. Contact angles of the mixed SAMs, on the other hand, were significantly different than those of pure SAMs and will be discussed below separately for each type of mixed SAM.

### 3.2.1. M1:M1C and M1:M9C mixed CT SAMs

In **Figure 3.2**, ellipsometric thickness and CAs of mixed M1:M1C films on TS-Au surfaces are presented as a function of the growth solution composition (mole ratio of M1 to M1C in the solution). In **Table 3.2**, CAs are summarized. CAs of mixed M1:M1C films are close to CAs of pure M1 SAMs for all mixtures. Even for 1:3 mixture, CAs of films are close to pure M1 SAMs. Hysteresis values for all mixtures of M1:M1C were similar to each other. Cassie's law was used to investigate that the correlation between the M1:M1C ratio that is 1:0 is corresponding pure M1 SAMs and 0:1 is corresponding pure M1C in the growth solution. To this end CAs of pure M1 and M1C SAMs were used in eq 2.6 in section 2.1.3 and the mole fraction of M1 on the surface (in the SAM)  $\chi_{M1,surf}$ , was calculated for each mixed SAM (that is, as a function of mole fraction of M1 in the growth solution,  $\chi_{M1,sol}$ ).

For surface composition analysis advancing contact angle values have been shown to give more reasonable results thus we based our analysis also on the advancing contact angles. It can be seen in **Figure 3.3** that for 1:1 solution ratio ( $\chi_{M1,sol} = 0.5$ ), the advancing CA yields a  $\chi_{M1,surf}$  value very close to 1. This indicates that the amount of M1 molecules on the surface is much higher than M1C molecules. Therefore, we can say that M1 has higher tendency to form film. In **Figure 3.3**, blue line represents the "ideal" case of  $\chi_{M1,sol} = \chi_{M1,surf}$ . If the surface fractions are assumed to be equal to the solution fractions, advancing contact angle values should follow the blue line but they lie above it. Hence, it can be concluded that M1 molecules binds to the gold surface stronger than M1C molecules. In **Figure 3.5**, ellipsometric thickness and CAs of mixed M1:M9C films on TS-Au surfaces are presented. In **Table 3.3**, CAs are summarized. It was observed that the CAs of mixed M1:M9C films are close to CAs of pure M1 SAMs for all mixtures. Even for 1:3 solution ratio, CA of the film is close to pure M1 SAM. According to contact angles results we can say that M1 molecules bind to Au surfaces more tightly than M9C molecules. In **Figure 3.6**, It can be seen that even for 1:3 M1:M9C solution ratio ( $\chi_{M9,sol} = 0.3$ ), the advancing CA yields an  $\chi_{M1,surf}$  value very close to 1 which shows that the amount of M1 molecules on the

surface is higher than M9C molecules. Nevertheless, a decreasing trend was observed in advancing contact angle values therefore we can conclude that M1 molecules bind to Au surfaces stronger than M1C and M9C molecules. The presence of a carboxyl functional group increases the steric demands of the molecules within the SAM, as was determined by the STM analysis [102], which may explain the difference in binding strengths of M1C, M9C and M1.

In **Figure 3.4** and **Figure 3.7**, AFM images of three different 1:1 ratio mixed M1:M1C and M1:M9C SAMs are shown. The morphology and roughness of the films are almost identical. All of the films possess a homogenous structure and no clear domain separation was observed in the phase images. Nevertheless, we should mention that AFM imaging of these samples were pretty difficult most probably due to the presence of carboxyl groups at the surface that strongly interact with water molecules in the ambient atmosphere and the ones reported in **Figure 3.4** and **Figure 3.7** are our best results. Hence for more credible conclusions AFM measurements in more controlled environment is necessary.

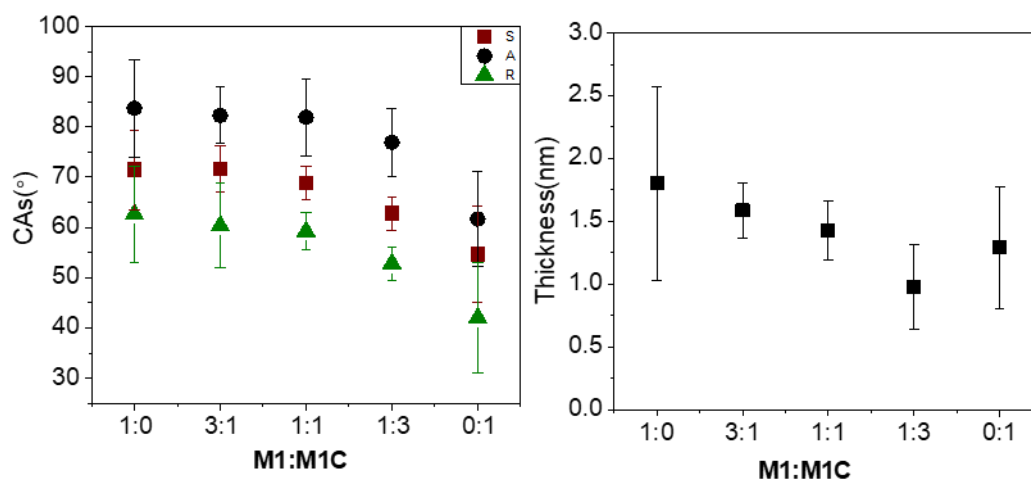


Figure 3-2 Contact angles and ellipsometric thicknesses of M1:M1C mixed SAMs as a function of growth solution mole ratio of M1 to M1C. S: static, A: advancing and R: receding contact angles

Table 3.2 Contact angles of M1:MIC mixed SAMs

<i>M1:MIC</i>	<i>Static</i>	<i>Advancing</i>	<i>Receding</i>	<i>Hysteresis</i>
<i>1:0</i>	71.5±8.0	83.7±9.7	62.7±9.6	21
<i>1:3</i>	62.8±3.3	76.9±6.7	52.8±3.3	24.1
<i>1:1</i>	68.9±3.2	81.9±7.7	59.2±3.7	22.7
<i>3:1</i>	71.6±4.7	82.3±5.6	60.4±8.4	21.9
<i>0:1</i>	54.7±9.7	61.7±9.4	42.0±11.0	19.7

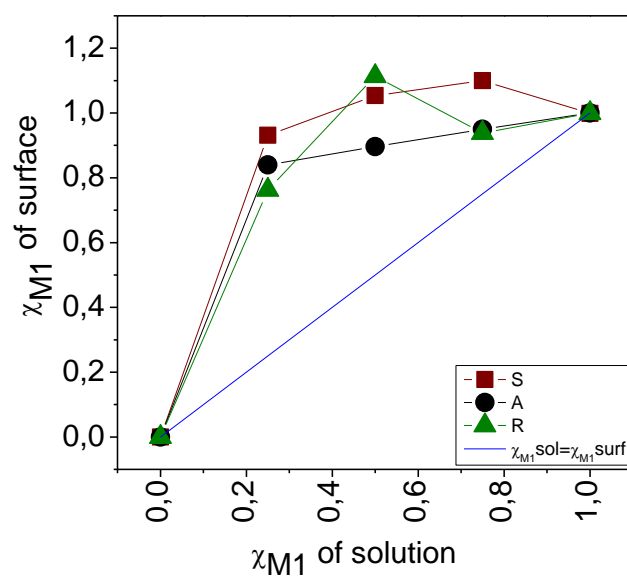


Figure 3-3 Surface composition of mixed M1:MIC SAMs calculated from the observed contact angles, plotted as a function of growth solution composition. S: static, A: advancing and R: receding contact angles.

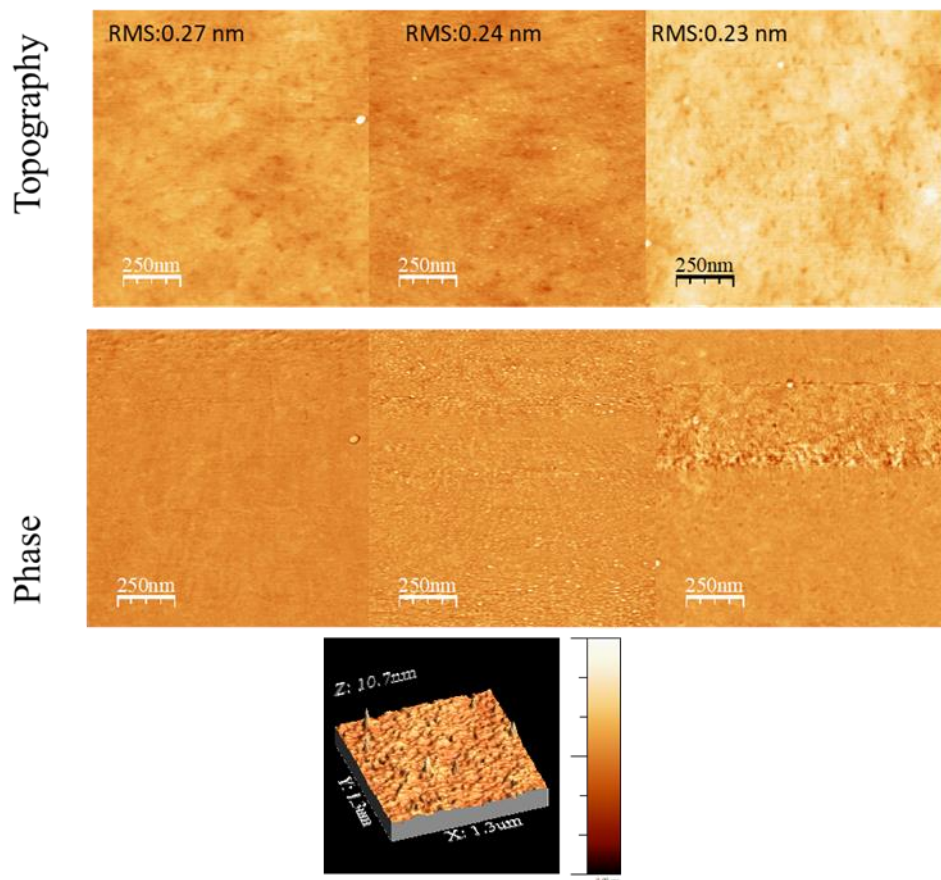


Figure 3-4 AFM images *M1:MIC (1:1)* mixed SAMs on template stripped gold surface. ( $1.25 \times 1.25 \mu\text{m}^2$ )

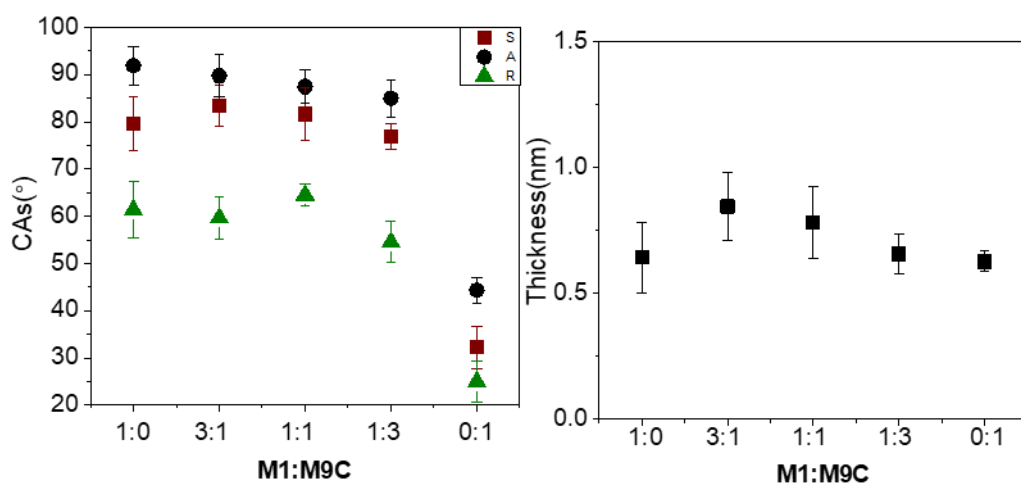


Figure 3-5 Contact angles and ellipsometric thicknesses of M1:M9C mixed SAMs. S: static, A: advancing and R: receding contact angles.

Table 3.3 Contact angles of M1:M9C mixed SAMs

<i>M1:M9C</i>	<i>Static</i>	<i>Advancing</i>	<i>Receding</i>	<i>Hysteresis</i>
<i>1:0</i>	79.6±5.7	91.9±4.1	61.4±5.9	30.5
<i>1:3</i>	76.9±2.7	85.0±4.0	54.5±4.4	30.5
<i>1:1</i>	81.7±5.4	87.4±3.6	64.5±2.4	22.9
<i>3:1</i>	83.4±4.4	89.7±4.4	59.7±4.4	30
<i>0:1</i>	32.3±4.5	44.4±2.7	25.0±4.4	19.4

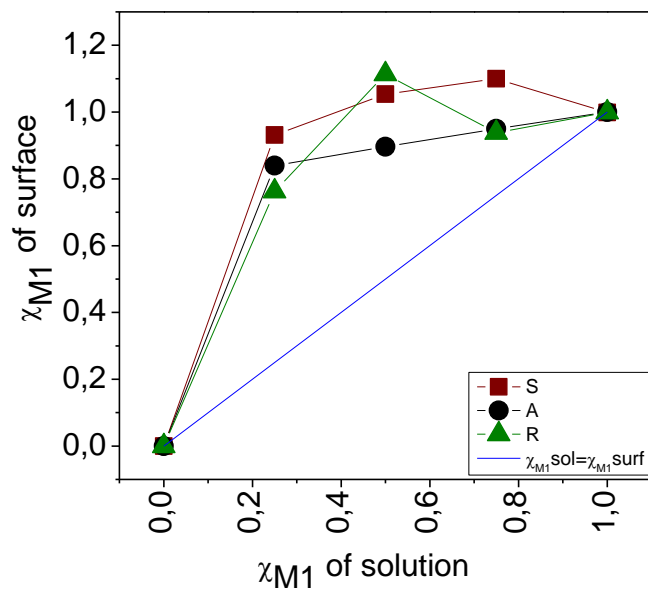


Figure 3-6 Surface composition of mixed M1:M9C SAMs calculated from the observed contact angles, plotted as a function of growth solution composition. S: static, A: advancing and R: receding contact angles.

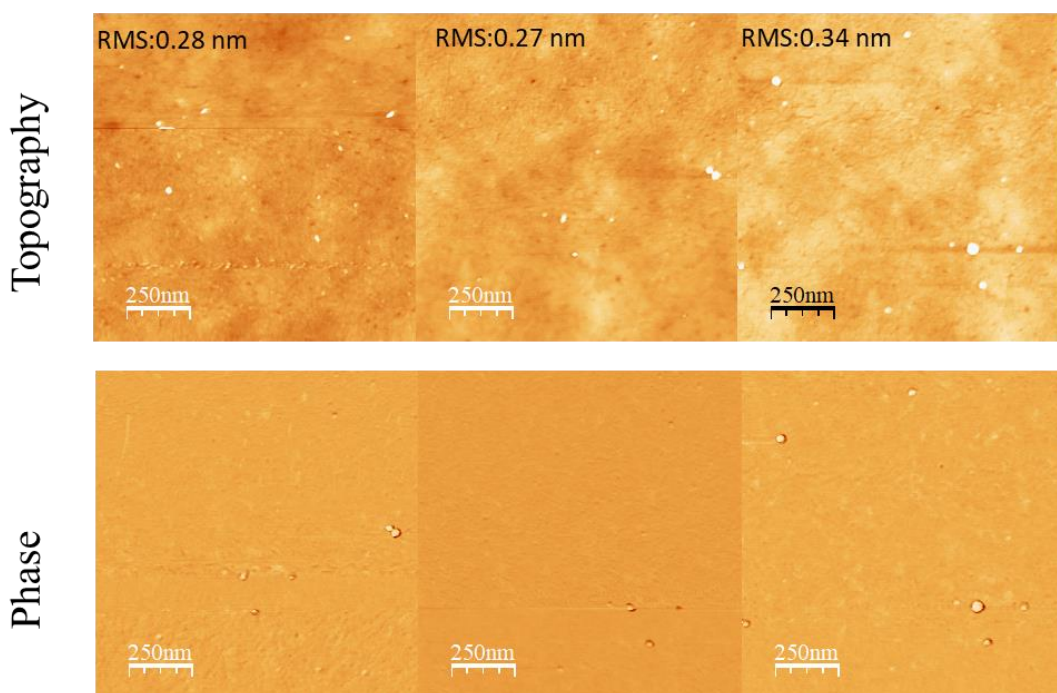


Figure 3-7 AFM images M1:M9C (1:1) mixed SAMs on template stripped gold surface. (1.25x1.25  $\mu\text{m}^2$ )

### 3.2.2. M9:M9C mixed CT SAMs

In Figure 3.8, ellipsometric thickness and CAs of mixed M9:M9C films on TS-Au surfaces are presented. In Table 3.4, CAs are summarized. It was observed that the CAs of mixed M9:M9C films are close to CAs of pure M9 SAMs for all mixtures and they seem to change randomly. Even for 1:3 solution ratio, CA of the film is very close to that of pure M9 SAM. Hysteresis values for all ratios of M9:M9C were similar to each other. According to contact angles results we can say that M9 molecules bind to Au surfaces stronger than M9C molecules. Cassie's law was used to investigate the correlation between the M9:M9C ratio in the growth solution and on the surface as detailed in the previous section. It can be seen in Figure 3.9 that for 1:3 M9:M9C solution ratio ( $\chi_{M9,sol} = 0.3$ ), the advancing CA yields an  $\chi_{M9,surf}$  value very close to 1 which indicates that the amount of M9 molecules on the surface is higher than M9C molecules. Therefore, we can say that M9 has higher tendency to form film. If the surface fractions are assumed to be equal to the solution fractions, advancing contact angle values should follow the blue line ( $\chi_{M9,sol} = \chi_{M9,surf}$ ) but they lie above it. It can be concluded that M9 molecules binds to the gold surface stronger than M9C molecules which may be due to higher steric demands of M9C.

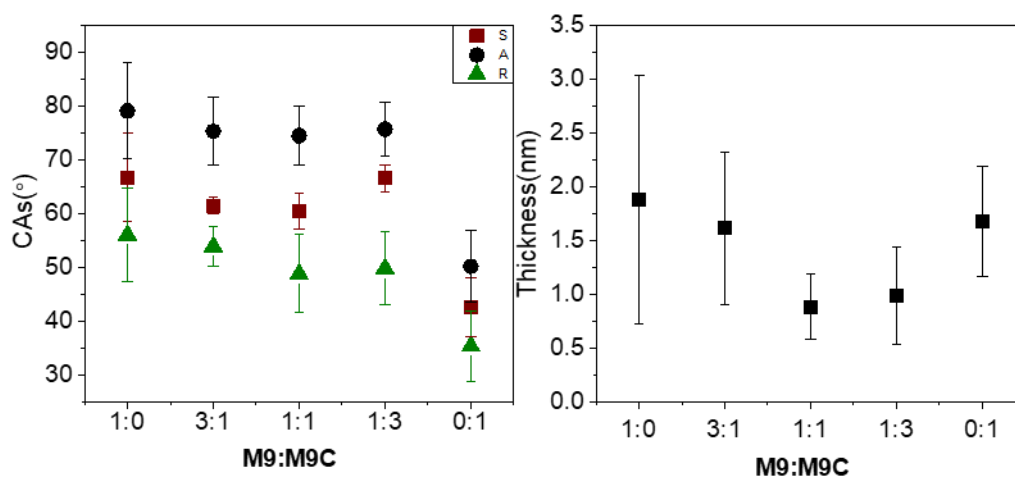


Figure 3-8 Contact angles and ellipsometric thicknesses of M9:M9C mixed SAMs as a function of growth solution mole ratio of M9 to M9C. S: static, A: advancing and R: receding contact angles.

Table 3.4 Contact angles of M9:M9C mixed SAMs

<i>M9:M9C</i>	<i>Static</i>	<i>Advancing</i>	<i>Receding</i>	<i>Hysteresis</i>
1:0	66.8±8.2	79.1±8.9	56.1±8.7	23
1:3	66.6±2.4	75.7±5.1	49.9±6.7	25.8
1:1	60.5±3.3	74.5±5.5	48.9±7.2	25.6
3:1	61.5±1.5	75.4±6.3	54.0±3.6	21.4
0:1	42.7±5.5	50.3±6.6	35.5±6.5	14.8

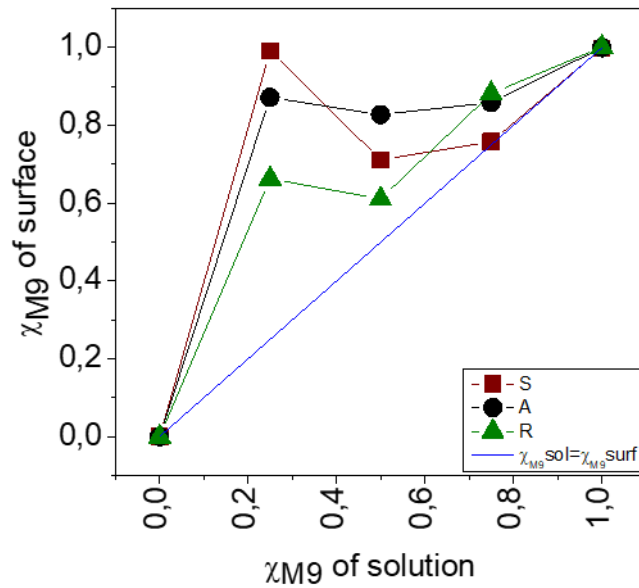


Figure 3-9 Surface composition of mixed M9:M9C SAMs calculated from the observed contact angles, plotted as a function of growth solution composition. S: static, A: advancing and R: receding contact angles.

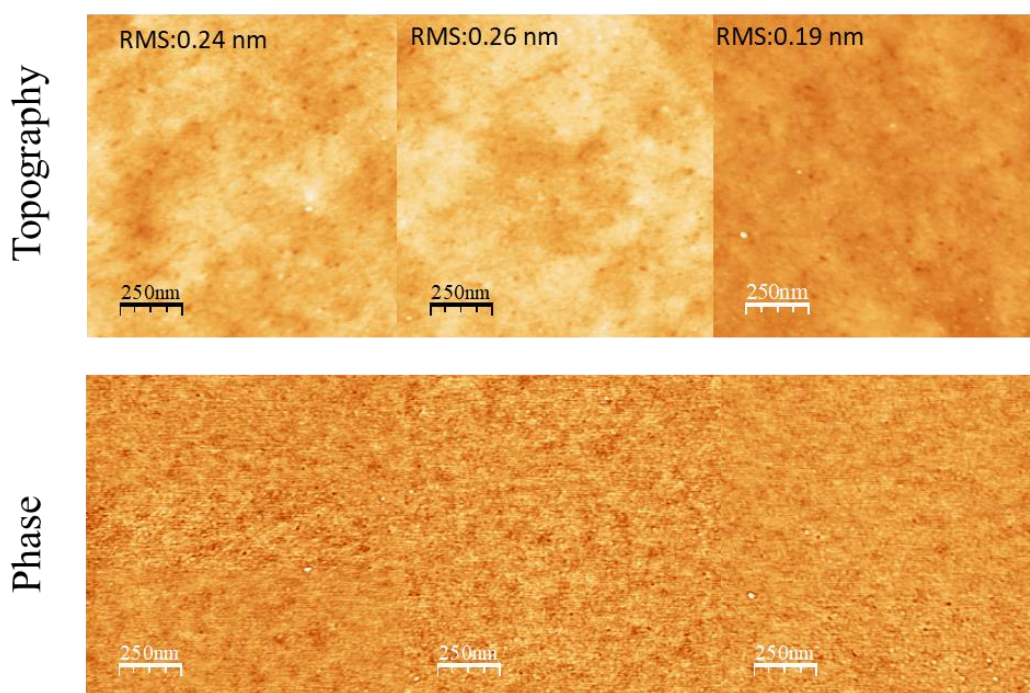


Figure 3-10 AFM images M9:M9C (1:1) mixed SAMs on template stripped gold surface. ( $1.25 \times 1.25 \mu\text{m}^2$ )

**In Figure 3.10**, AFM images of three different 1:1 ratio mixed M9:M9C SAMs are shown. Similar to mixed M1:M1C SAMs, the topography of the films are almost identical. All of the films have a homogenous morphology resulting in very similar phase images. Therefore, it is not possible to extract surface properties from phase images. Moreover, as we mentioned before, AFM imaging is very difficult with these samples, due to the presence of carboxyl groups at the surface. Thus, it is necessary to conduct more sensitive AFM measurement and data analysis.

### 3.2.3. M9:M1C mixed CT SAMs

**In Figure 3.11**, ellipsometric thickness and CAs of mixed M9:M1C films on TS-Au surfaces are presented. **In Table 3.5**, CAs are summarized. It was observed that the CAs of mixed M9:M1C films are close to CAs of pure M9 SAMs for all ratios. Even for 1:3 solution ratio, CA of film is close to pure M9 SAM. Hysteresis values for all ratios of M9:M1C in growth solution were similar to each other. According to contact angles results we can say that M9 molecules bind to Au surfaces more tightly than M1C molecules. In the case of M9:M1C mixtures, due to the small difference between

the contact angles of pure M1C and M9 films, Cassie's law could be reliably applied only to advancing contact angles as shown **Figure 3.12**. It can be seen in **Figure 3.12** that for 1:3 M9:M1C solution ratio ( $\chi_{M9,sol} = 0.3$ ), the advancing CA yields an  $\chi_{M9,surf}$  value is very close to 1 which indicates the amount of M9 molecules on the surface to be higher than M1C molecules. Therefore, we can conclude that M9 has higher tendency to form film.

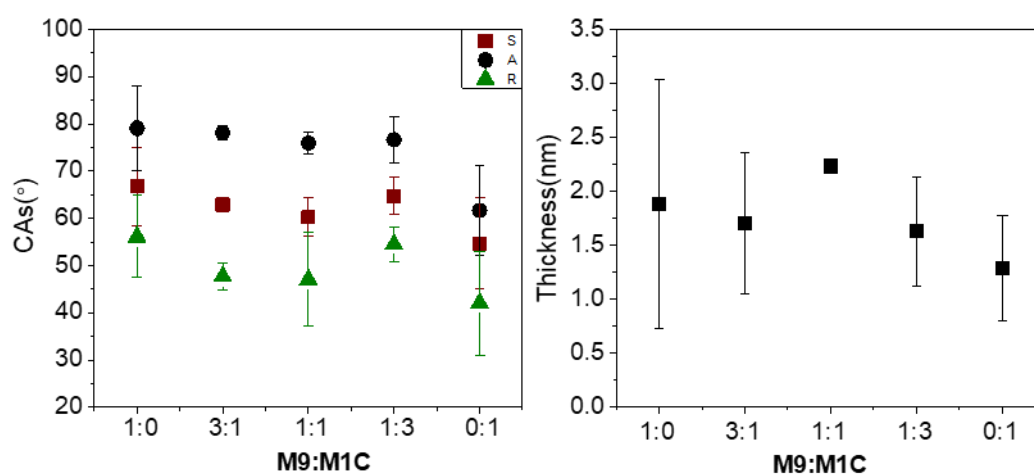


Figure 3-11 Contact angles and ellipsometric thicknesses of M9:M1C mixed SAMs. S: static, A: advancing and R: receding contact angles.

Table 3.5 Contact angles of M9:M1C mixed SAMs

<i>M9:M1C</i>	<i>Static</i>	<i>Advancing</i>	<i>Receding</i>	<i>Hysteresis</i>
<i>1:0</i>	66.8±8.2	79.1±8.9	56.1±8.7	23
<i>1:3</i>	64.7±4.0	76.7±4.9	54.5±2.9	22.2
<i>1:1</i>	60.2±4.1	75.9±2.4	47.1±9.9	28.8
<i>3:1</i>	62.9±1.4	78.1±1.6	47.7±3.6	30.4
<i>0:1</i>	54.7±9.7	61.7±9.4	42.0±11.0	19.7

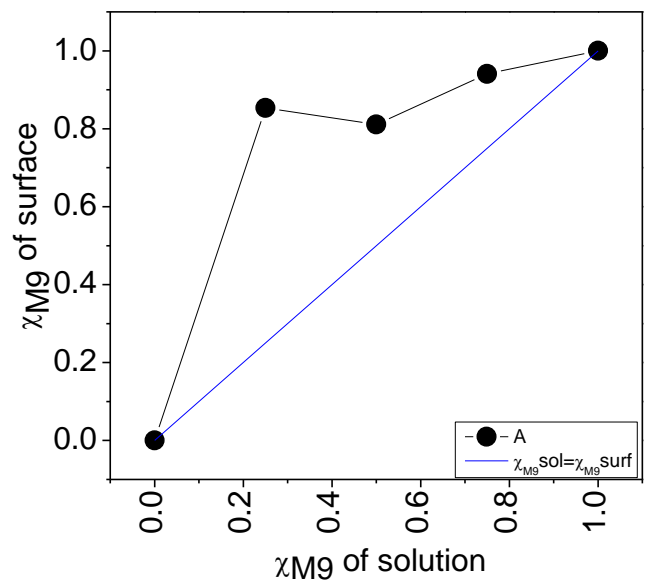


Figure 3-12 Surface composition of mixed M9:MIC SAMs calculated from the observed contact angles, plotted as a function of growth solution composition. S: static, A: advancing and R: receding contact angles.

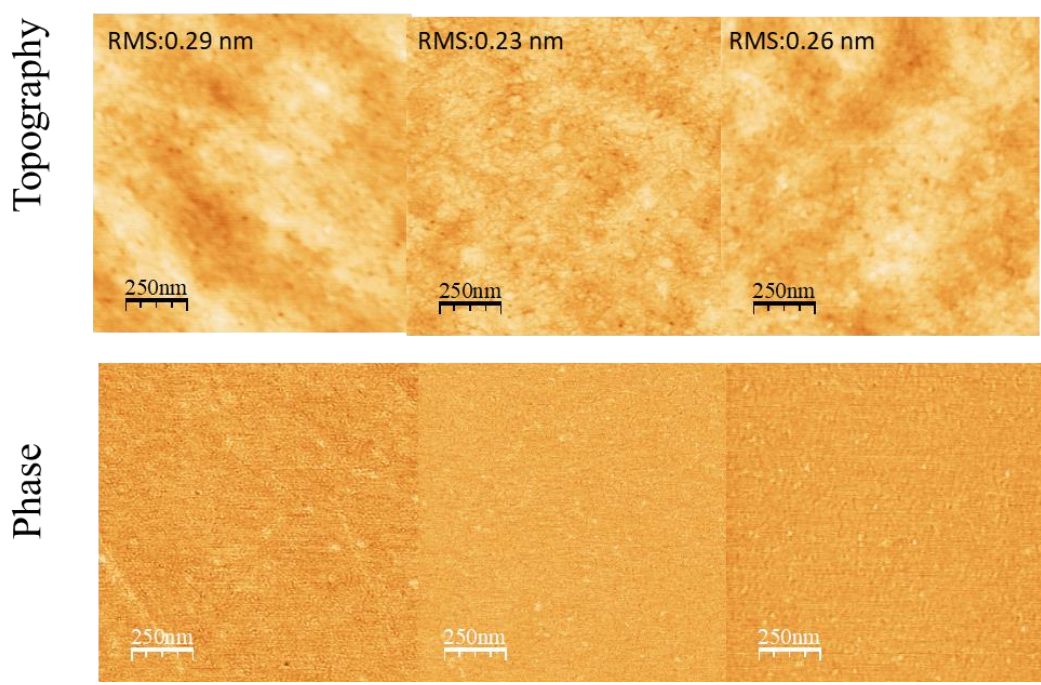


Figure 3-13 AFM images M9:MIC (1:1) mixed SAMs on template stripped gold surface. (1.25x1.25  $\mu\text{m}^2$ )

In **Figure 3.13**, AFM images of three different 1:1 ratio mixed M9:M1C SAMs are shown. Similar to previous mixed CT SAMs, the surface morphology of the films are very similar and indiscernible. In our measurements, we observed that there is no surface property that may cause surface phase lag on the surface, therefore all of the films have almost the same phase images. Due to the previously mentioned difficulty in AFM imaging with these samples it is required to perform more sensitive AFM measurement and data analysis.

In **Figure 3.14**, surface composition of all mixed SAMs calculated from the observed advancing contact angles is plotted as a function of growth solution composition. M9:M9C and M9:M1C results are very close to each other therefore changing the position of sulfur group does not affect the results significantly. On the other hand, M1:M1C and M1:M9C results are slightly different than each other thus M1 molecules can be concluded to have different interaction with M1C and M9C. In addition, for all the investigated mixed SAMs morphology of the films were almost identical with average roughness values of about 0.3 nm.

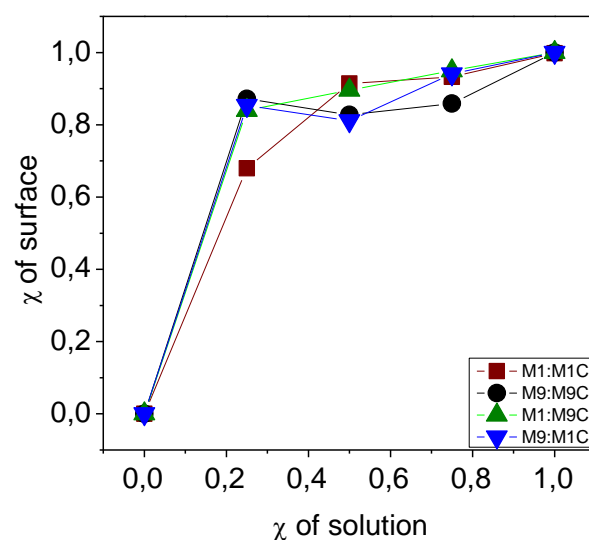


Figure 3-14 Calculated surface composition of all mixed SAMs based on advancing contact angles, plotted as a function of growth solution composition.

### 3.3. Replacement Experiments

In this part of the study we performed replacement experiments by keeping a pure CT SAM in the growth solution of another CT molecule. To this end, four different type of experiments were carried out: Pure M1 SAMs were kept in M9C solution, pure M9C SAMs were kept in M1 solution, pure M9 SAMs were kept in M1C solution and finally pure M1C SAMs were kept in M9 solution for 5 days and the contact angles and thicknesses were measured daily. Firstly, control experiments were performed before the replacement experiments to check the stability of the pure SAMs in ethanol for an extended period.(5 day) the results of which are shown in **Figure 3.15**. After 5 days, the contact angle for pure SAMs did not change significantly if we consider the errors. Based on these results, it can be concluded that molecules in the SAMs do not desorb significantly in 5 days.

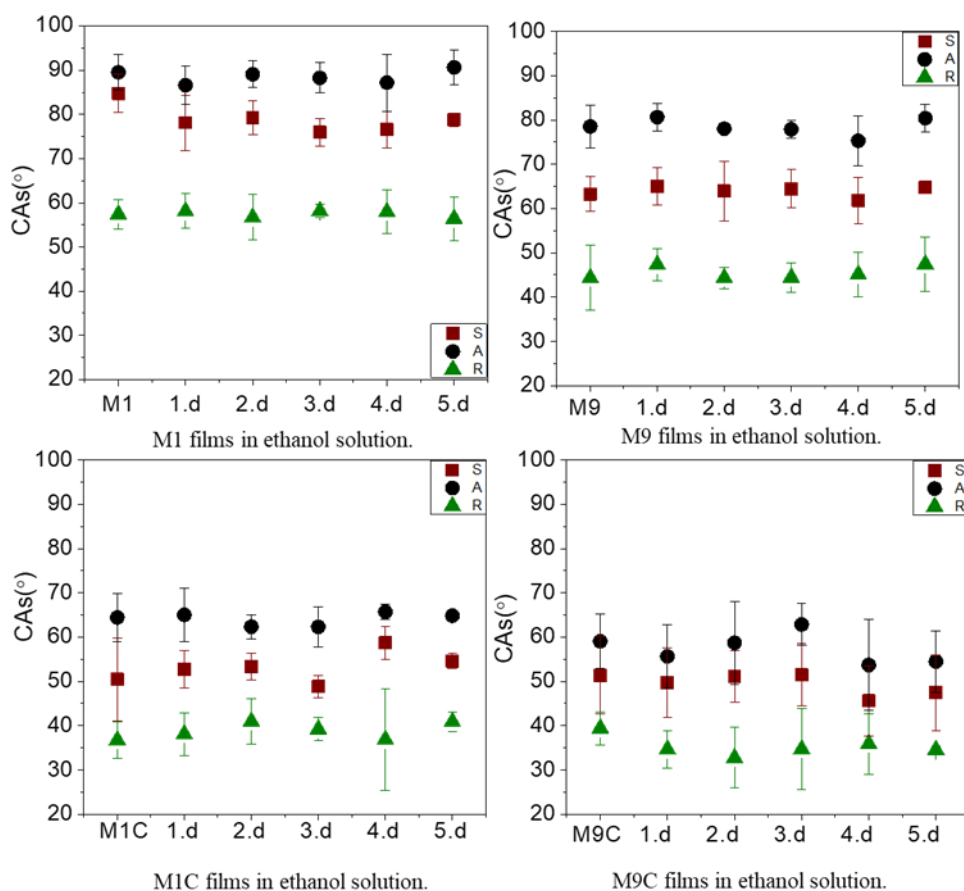


Figure 3-15 Control experiments of pure SAMs in ethanol solution.

### 3.3.1. M1 films in M9C solution and M9C films in M1 solution

In Figure 3.16, ellipsometric thickness and CAs of M1 films in M9C solution are presented. In Table 3.6, CAs are summarized. When the advancing CAs in Figure 3.15 are examined a slow decay can be observed which indicates that some of the M1 molecules on the surface were replaced by M9C molecules. However, this replacement is limited and even after 5 days in the M9C growth solution the advancing CAs decreased only about 10 degrees, which indicates that the major component on the surface (in the SAM) was still M1. To perform a more quantitative analysis of the surface composition change as a function of the time period that the pure M1 SAM spent in the M9C solution, we employed Cassie's law and calculated the M1 mole

fraction on the surface. According to this analysis, shown in **Figure 3.17**, mole fraction of M1 was 0.93 after one day and decreased to 0.72 at fifth day. Based on this results it can be concluded that after 5 days M9C replaces only 28% of the M1 molecules in the pure M1 SAM. **In Figure 3.18**, ellipsometric thickness and CAs of M9C films in M1 solution are presented. **In Table 3.7**, CAs are summarized. When the advancing contact angles of M1 films in **Figure 3.18** are examined, a clear increasing trend can be observed (with a rise of about fifteen degree at the end 5 days). Hence, M9C molecules on the surface were replaced by M1 molecules significantly. **In Figure 3.19**, surface coverage was calculated by using Cassie's law. According to this analysis, mole fraction of M9C was 0.95 at first day and decreased to 0.52 after 5 days of waiting. Based on these results it can be concluded that after 5 days M1 replaces almost half (48%) of the M9C molecules in the pure M9C SAM. When compared with results provided in the previous section, this indicates that M1 replaces M9C much faster than M9C replaces M1. This observation which implies M1 to have higher tendency to bind to the gold surface is in agreement with the results of the mixed SAM experiments discussed in **section 3.2**.

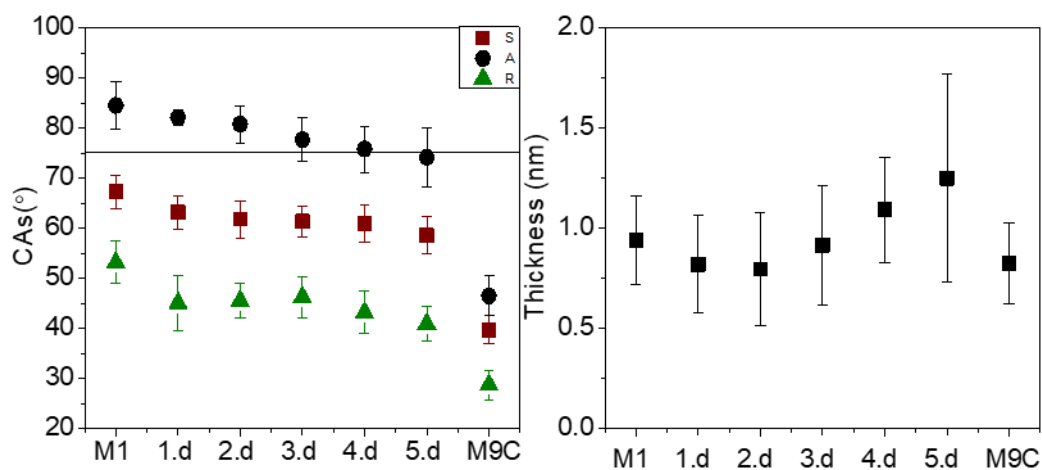


Figure 3-16 Contact angle measurements and ellipsometric thickness of M1 films in M9C solution. S: static, A: advancing and R: receding contact angles

Table 3.6 Contact angles of M1 films in M9C solution replacement experiment.

<i>M1 films in M9C sol</i>	<i>Static</i>	<i>Advancing</i>	<i>Receding</i>	<i>Hysteresis</i>
<i>M1</i>	67.3±3.3	84.5±4.5	53.2±4.2	31.3
<i>1.d</i>	63.2±3.3	82.1±1.6	45.1±5.4	37
<i>2.d</i>	61.8±3.7	80.8±3.7	45.6±3.4	35.2
<i>3.d</i>	61.4±3.1	77.7±4.4	46.3±4.0	31.4
<i>4.d</i>	61.0±3.8	75.8±4.6	43.2±4.2	32.6
<i>5.d</i>	58.6±3.7	74.2±6.0	41.0±3.5	33.2
<i>M9C</i>	39.8±2.8	46.5±4.0	28.8±2.9	17.7

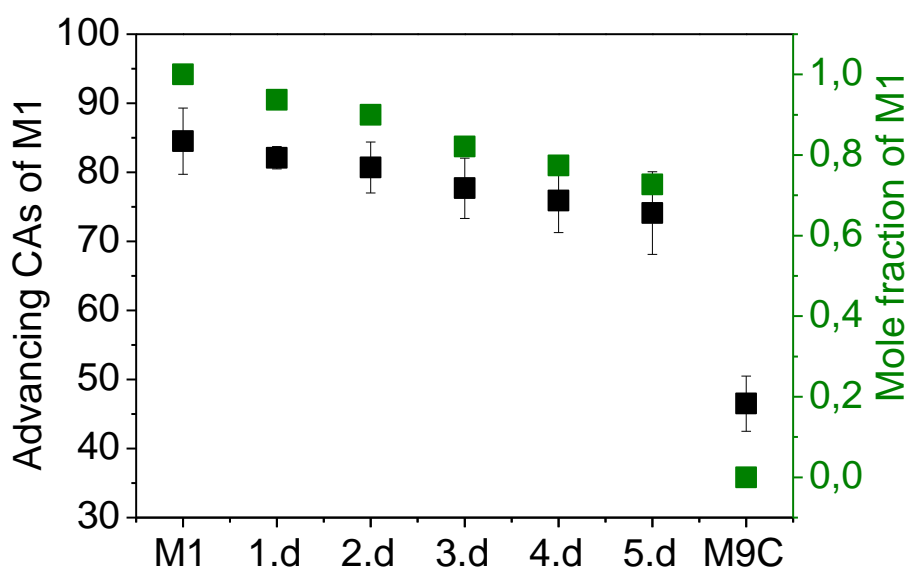


Figure 3-17 Surface coverage of M1 films in M9C solution experiment.

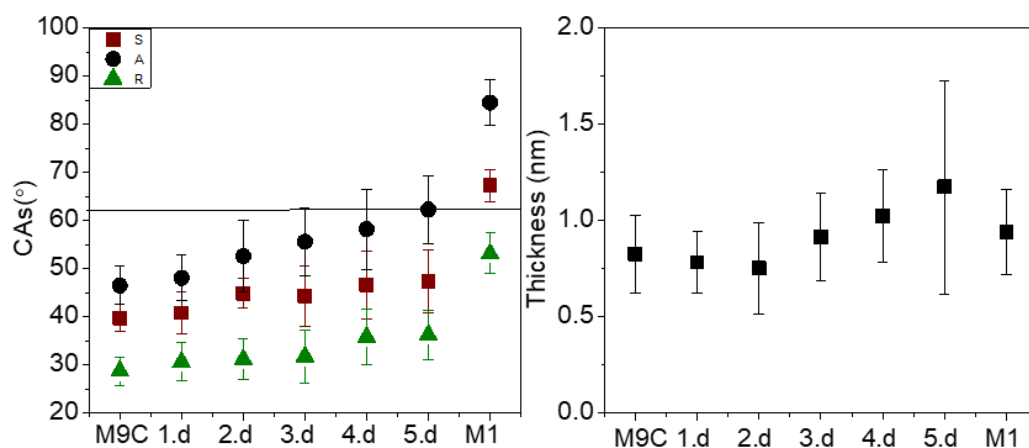


Figure 3-18 Contact angle measurements and ellipsometric thickness of M9C films in M1 solution SAMs. S: static, A: advancing and R: receding contact angles.

Table 3.7 Contact angles of M9C films in M1 solution replacement experiment.

<i>M9C films in M1 sol</i>	<i>Static</i>	<i>Advancing</i>	<i>Receding</i>	<i>Hysteresis</i>
<i>M9C</i>	39.8±2.8	46.5±4.0	28.8±2.9	17.7
<i>1.d</i>	40.8±4.3	48.1±4.7	30.7±3.9	17.4
<i>2.d</i>	44.9±3.1	52.6±7.5	31.2±4.2	21.4
<i>3.d</i>	44.4±6.4	55.6±7.1	31.8±5.5	23.8
<i>4.d</i>	46.7±7.0	58.2±8.3	35.9±5.7	22.3
<i>5.d</i>	47.4±6.5	62.3±7.0	36.3±5.1	26
<i>M1</i>	67.3±3.3	84.5±4.8	53.2±4.2	31.3

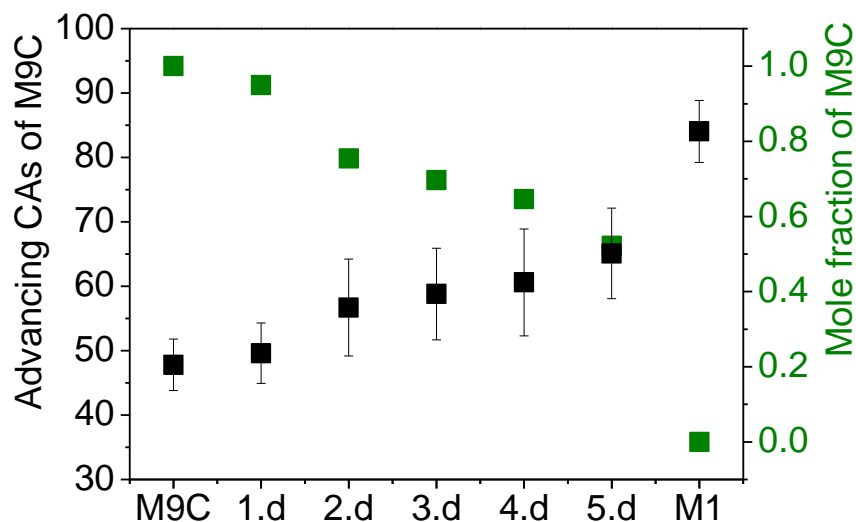


Figure 3-19 Surface coverage of M9C films in M1 solution experiment.

### 3.3.2. M9 films in M1C solution

In Figure 3.20, ellipsometric thickness and CAs of M9 films in M1C solution are presented. In Table 3.8, CAs are summarized. When the static and receding CAs in Figure 3.20 are examined a slow decay can be observed which indicates that some of the M9 molecules on the surface were replaced by M1C molecules. However, this replacement is limited and even after 5 days in the M1C growth solution the static CAs decreased only about 6 degrees, which indicates that the major component on the surface (in the SAM) was still M9. To perform a more quantitative analysis of the surface composition change as a function of the time period that the pure M9 SAM spent in the M1C solution, we employed Cassie's law and calculated the M9 mole fraction on the surface. According to this analysis shown in Figure 3.21, mole fraction of M9 was 0.90 after one day and decreased to 0.73 after 5 days. Based on these results it can be concluded that after 5 days M1C replaces only 27% of the M9 molecules in the pure M9 SAM.

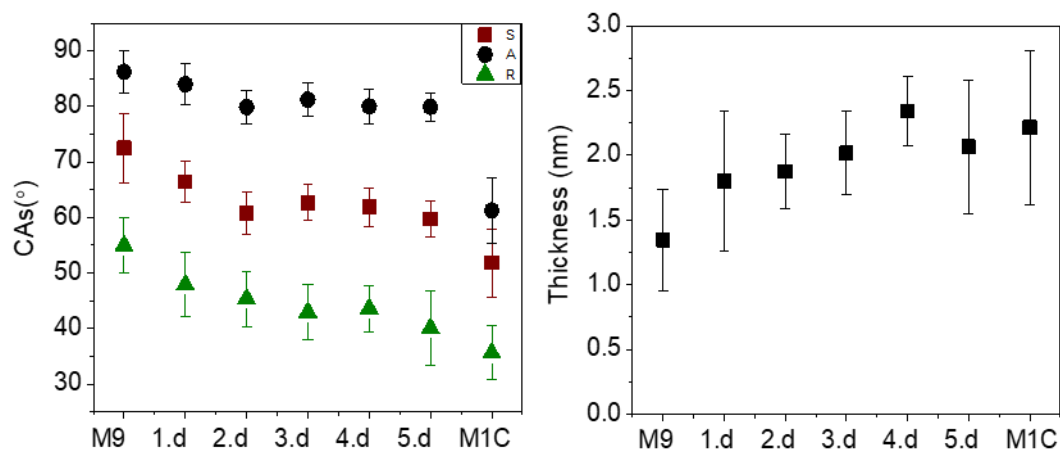


Figure 3-20 Contact angle measurements and ellipsometric thickness of M9 films in MIC solution SAMs. S: static, A: advancing and R: receding contact angles.

Table 3.8 Contact angles of M9 films in MIC solution replacement experiment

<i>M9 films in MIC sol</i>	<i>Static</i>	<i>Advancing</i>	<i>Receding</i>	<i>Hysteresis</i>
<i>M9</i>	72.5±6.3	86.2±3.8	55.0±5.0	31.2
<i>1.d</i>	66.4±3.7	84.0±3.8	47.9±5.7	36.1
<i>2.d</i>	60.8±3.9	79.9±3.0	45.4±5.0	34.5
<i>3.d</i>	62.6±3.2	81.2±3.0	42.9±5.0	38.3
<i>4.d</i>	61.9±3.5	80.0±3.1	43.6±4.2	36.4
<i>5.d</i>	59.7±3.3	79.9±2.5	40.1±6.8	39.7
<i>MIC</i>	51.8±6.1	61.3±5.9	35.6±4.8	25.7

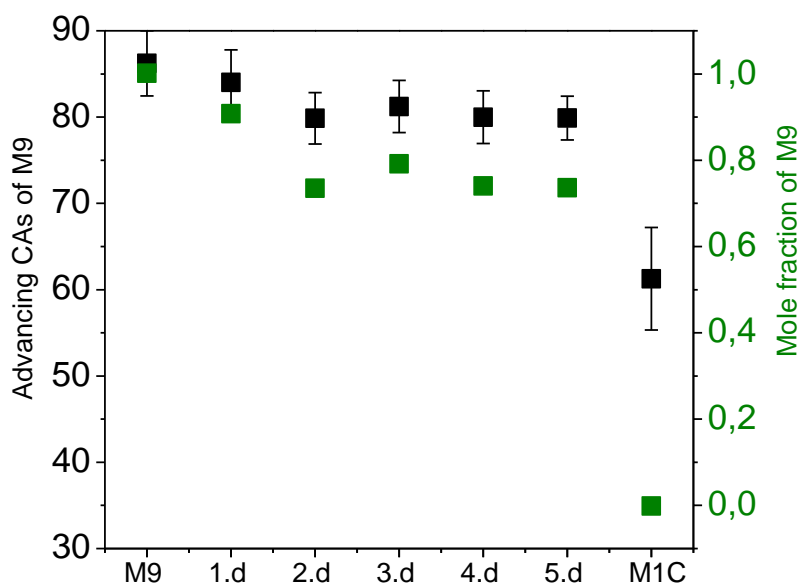


Figure 3-21 Surface coverage of M9 films in M1C solution experiment.

### 3.3.3. M1C films in M9 solution

In Figure 3.22, ellipsometric thickness and CAs of M9 films in M1C solution are presented. In Table 3.9, CAs are summarized. When the CAs in Figure 3.22 are examined, we observe an unexpected behavior in all CAs. We expect CAs of resulting film to be in between the CAs of M1C and M9. In the previous section, we see that M1C replaces M9 molecules in the pure M9 SAMs only partially. Considering this, here, we expect M9 to replace M1C molecules in the pure M1C film significantly. Consequently, CAs of the M1C film should increase over time. However, CAs are even lower than both pure SAMs. Lower CAs indicate that resulting film is even more hydrophilic than pure M1C SAM. This very interesting result will be discussed further in section 3.4.2.

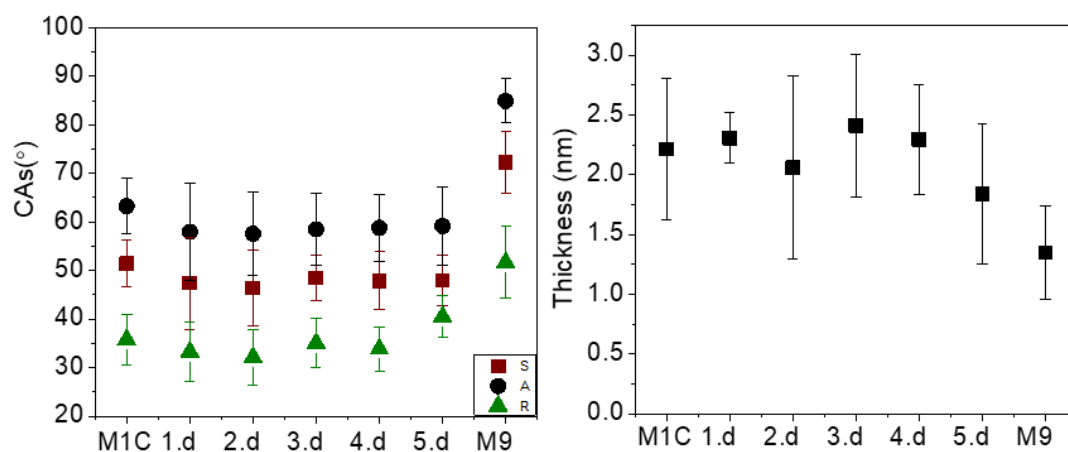


Figure 3-22 Contact angle measurements and ellipsometric thickness of MIC films in M9 solution SAMs. S: static, A: advancing and R: receding contact angles

Table 3.9 Contact angles of MIC films in M9 solution replacement experiment

<i>MIC films in M9 sol</i>	<i>Static</i>	<i>Advancing</i>	<i>Receding</i>	<i>Hysteresis</i>
<i>MIC</i>	51.8±6.1	61.3±5.9	35.6±4.8	25.7
<i>1.d</i>	35.8±3.3	45.7±3.6	28.5±2.9	17.2
<i>2.d</i>	40.1±2.9	49.8±2.7	28.4±2.7	21.4
<i>3.d</i>	44.4±3.0	50.7±4.0	32.0±4.7	18.7
<i>4.d</i>	41.2±3.2	50.8±3.4	32.0±2.1	18.8
<i>5.d</i>	43.7±3.1	51.2±2.2	29.0±2.2	22.2
<i>M9</i>	72.5±6.3	86.2±3.8	55.0±5.0	31.2

### 3.4. Replacement Experiments on Ag surfaces

In order to compare the behavior of CT molecules on gold surface with their behavior on silver surface and to have an idea of the interaction of carboxyl functionalized CTs with oxide surfaces we repeated replacement experiments on template stripped silver surfaces. The results of these measurements will be discussed below.

### 3.4.1. M1 films in M9C solution and M9C films in M1 solution

In **Figure 3.23 A-B**, CAs of M1 films in M9C solution and M9C films in M1 solution are presented. The corresponding surface composition plots are shown in **Figure 3.24 A-B**. When these two figures are examined, it can be seen that M9C replaces M1 very quickly and completely. On the other hand, though M1 replaces M9C as well, this replacement is much slower and takes place only to a limited extent. This is most probably due to M9C adsorbing on the oxidized regions of the silver surface through carboxylic group strongly, whereas, M1 adsorbing on the unoxidized regions through sulfur atoms rather weakly. Since silver readily oxidizes in air, it is normal for our template stripped silver surfaces to have a very high coverage of oxidized regions. In fact, in the literature, Zharnikov research group studied chemisorption of 16-mercaptohexadecanoic ( $\text{COOH}(\text{CH}_2)_{15}\text{SH}$ ) acid on indiumtin oxide (ITO) surface by using XPS and they found bifunctional acids to adsorb on ITO surface via carboxylic group resulting in thiol terminated SAMs [103].

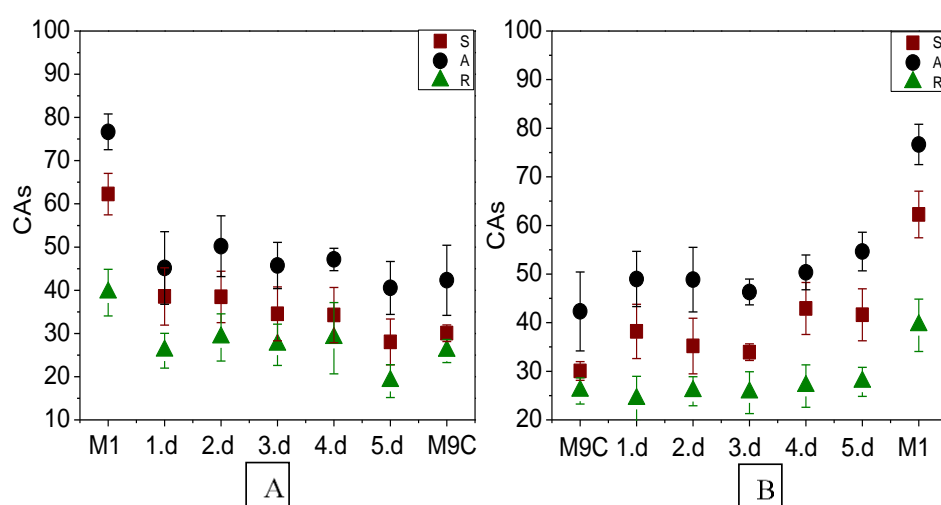


Figure 3-23 A) Contact angle measurements of M1 films in M9C solution and B) Contact angle measurements of M9C films in M1 solution respectively. S: static, A: advancing and R: receding contact angles.

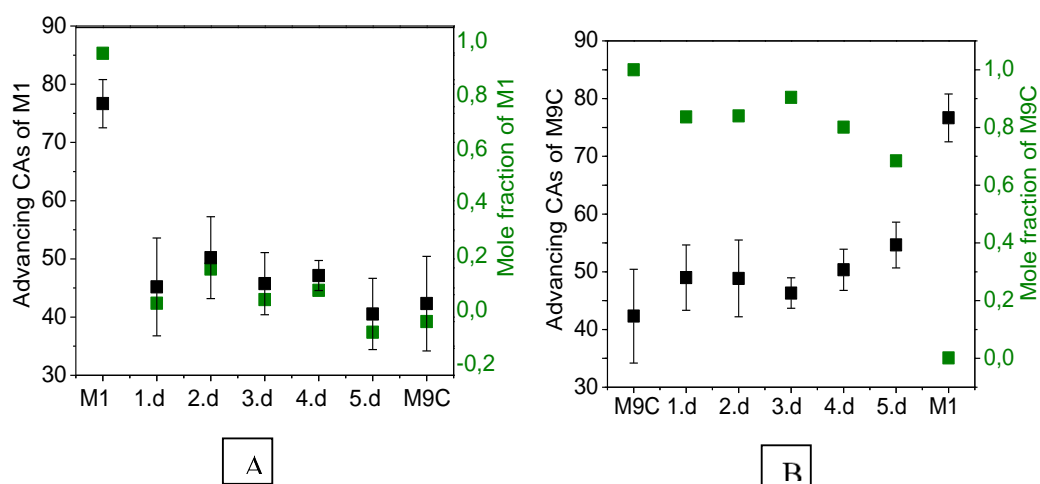


Figure 3-24 A) Surface coverage of M1 films kept in M9C solution. B) Surface coverage of M9C films kept in M1 solution.

### 3.4.2. M9 films in M1C solution and M1C films in M9 solution

In **Figure 3.25 A-B**, CAs of M9 films kept in M1C solution and M1C films kept in M9 solution are presented. Interestingly on the silver surface pure M9 and M1C films have similar contact angle values, hence performing a Cassie's law calculation for determining the surface composition in replacements measurements is not possible. More interestingly, however, in the case of M1C films kept in M9 solution, immediately on the first day of the measurement CA values decrease significantly and stay more or less constant with increasing waiting period (of the film in M9 solution). This, very interesting situation, is similar to what is observed during the replacement measurements of M1C films kept in M9 solution on TS-Au (section 3.3.4). Observation of similar behavior on two different surfaces (gold and silver) indicates that this “weird” phenomenon is not an artifact but due to interaction of M9 molecules in the growth solution with the M1C molecules in the SAM. Due to this special interaction, M1 molecules may be assisting the M1C molecules in the SAM to reorganize in a way that carboxylic acid group are more exposed on the SAM surface resulting in lower contact angles. Nevertheless, these results need more reproducibility

tests, since we could perform the replacement measurements reported in the section and in section 3.3.4 only twice (though on three parallel samples).

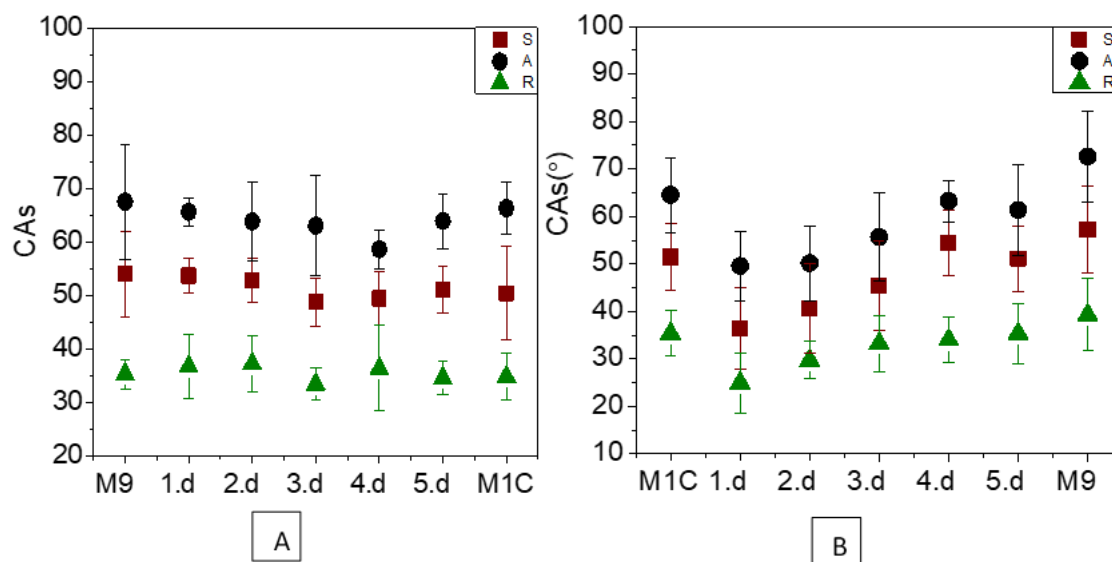
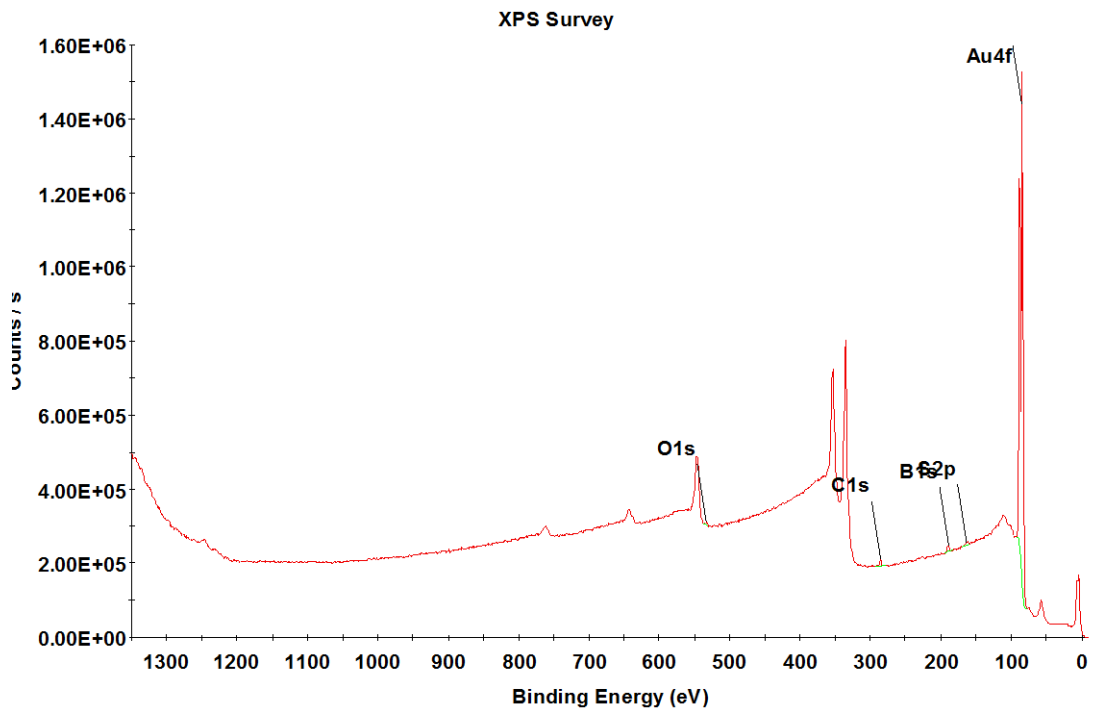


Figure 3-25 Contact angle values of (A) M9 films kept in MIC solution and (B) MIC films kept in M9 solution.

### 3.5. X-Ray photoelectron spectroscopy results

To confirm the conclusions derived based on contact angle measurements we performed XPS measurements on some of the CT SAMs. Due to funding, time and technical limitations we could study only 1 samples of pure M1 SAM, 1 samples of pure M9C SAM, 1 samples of 1:1 solution ratio M1:M9C mixed SAM and finally 1 sample (each) of pure M1 SAM kept in M9 solution for 1, 2 and 3 days. Representative survey and elemental scans are shown in **Figure 3.26** and **Figure 3.27** (rest of the raw data is provided in the appendix).



*Figure 3-26 Survey scan of M1 film.*

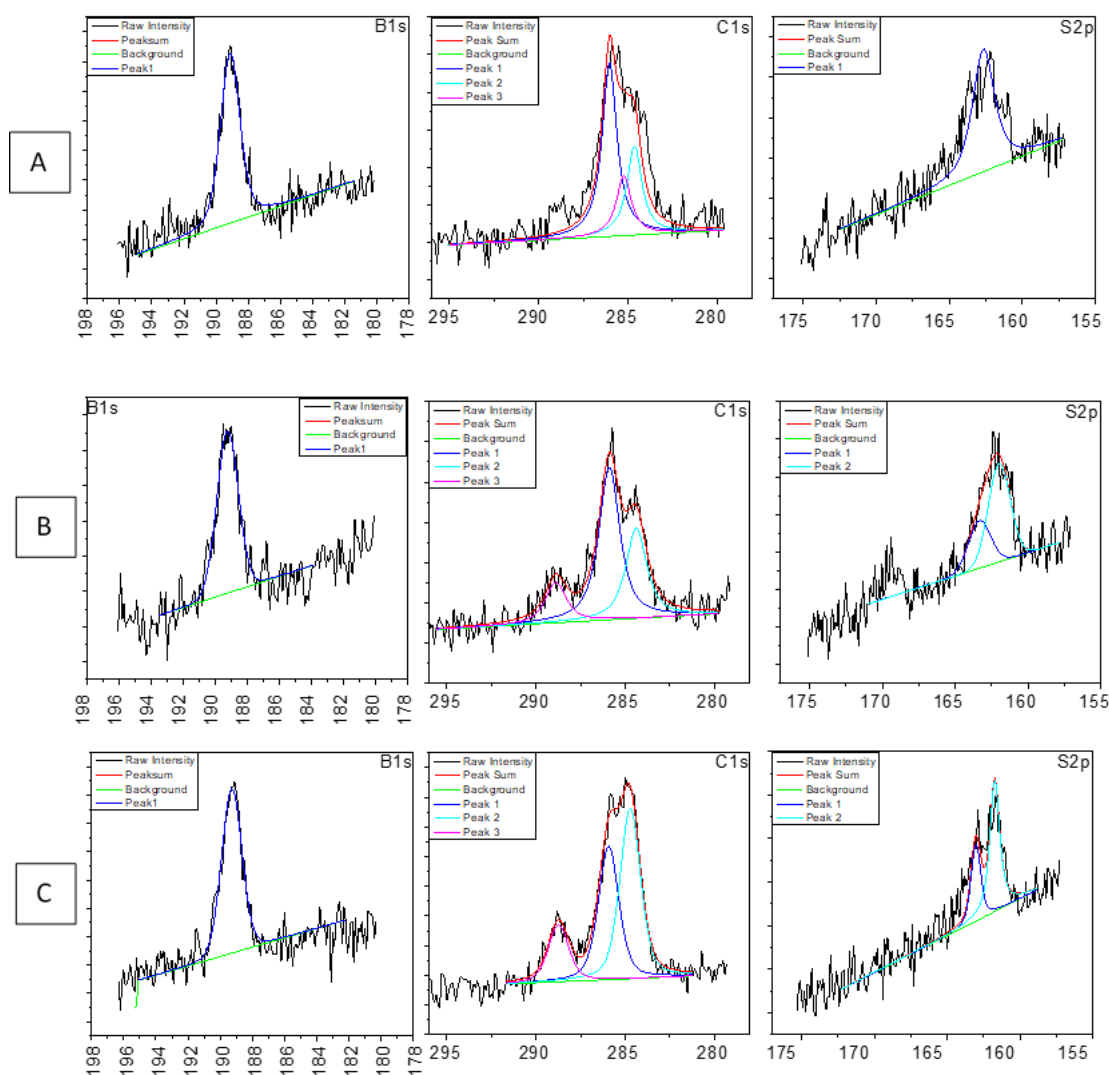


Figure 3-27 Peak fitting process for A) M1, B) 1:1 mixture of M9C and M1, C) M9C obtained from using XPS Peak Fit software.

In **Table 3.11**, measured core level binding energies and Full-Width Half-Maximum (FWHM) of S 2p<sub>3/2</sub>, C 1s and B 1s peaks for these samples are tabulated. The measured BE value of S 2p electrons is comparable to the value reported in the literature [52–54] for alkanethiolates on gold surfaces. The spectra of C 1s photoelectrons were fit by three components of the same width with binding energies

of about 284.6, 285.8, and 288.8 eV, which can be assigned to carbon atoms with  $-C-H$  (first component),  $-C-B$  (second component) and  $-COO$  (third component, present only in M9C) bonds. For M1, the spectra of C 1s photoelectrons were fit by three components of the same width with binding energies of about 284.6, 285.8, and 285.2 eV, which can be assigned to carbon atoms with  $-C-H$  (first component),  $-C-B$  (second component) and  $-C-S$  (third component), bonds [98]. In **Table 3.10**, the third component which is coming from carboxylic function is not present for pure M1 SAMs as expected. In **Table 3.11**, atomic concentrations of elements relative to the concentration of boron atoms (=10) are given. For M9C films, we expect that when the boron concentration is fixed to 10, the sulfur, carbon, and oxygen concentrations should be 1, 3, and 2, respectively. Sulfur, oxygen and carbon concentrations were found to be higher than the expected concentration. We attributed this result to contamination and presence of physisorbed CTs on the SAM surface. In **Table 3.11**, for third carbon component,  $-COO$ , there is increasing trend for M1 films kept in M9C solution as the waiting period increases which is in agreement with our expectation based on contact angle measurements. Though, total oxygen concentration increases with waiting period of M1 in M9C, the contribution of carboxyl oxygens to this increase could not be determined conclusively based on XPS fits. For XPS measurements, replacement experiment was not conducted with standard procedure (detailed in section 3.3). In order to make the measurement all at once, we prepared the samples beforehand and we used 3 different samples prepared on different days. Since the samples were prepared and transferred under ambient conditions, consequently some uneven carbonaceous contamination exist for different samples.

Table 3.10 Measured Core Level Binding Energies and FWHM of M9C films in M1 solution.

	S2p	FWHM	B1s	FWHM	C1s	FWHM	O1s	FWHM
M1-1	162.6	1.8	189.1	1.4	286.0	1.0	532.2	1.4
					284.6	1.0		
					285.2	1.0		
1:1-Mix-1	161.9	1.8	189.2	1.6	285.8	1.4	531.4	1.4
	163.3	1.8			284.3	1.4	532.5	1.4
					288.8	1.4		
M9C-1	161.7	0.8	189.3	1.5	285.9	1.4	531.7	1.4
	163.0	0.8			284.7	1.4	532.7	1.4
					288.7	1.4		
1.d	162.1	1.3	189.1	1.5	285.9	1.6	531.5	1.4
	163.5	1.3			284.6	1.6	532.6	1.4
					288.8	1.6		
2.d	162.1	1.3	189.1	1.5	285.9	1.5	531.5	1.4
	163.6	1.3			284.6	1.5	532.7	1.4
					288.8	1.5		
3.d	162.2	1.3	189.2	1.6	285.9	1.5	531.5	1.4
	163.7	1.3			284.2	1.5	532.1	1.5
					288.9	1.5		

Table 3.11 Atomic Concentrations of Elements on Au Surfaces Relative to the Concentration of Boron Atoms (=10) As Determined from XPS Analyses Assuming Homogeneous Samples

	S2p	B1s	C1s total	O1s	Au4f	C-H	C-B	C-OO	C-S
M1-1	1.8	10.0	6.8	1.3	39.2	1.9	3.7	0.0	1.3
1:1-Mix-1	2.2	10.0	9.5	4.4	50.4	3.0	5.1	1.4	
M9C-1	1.3	10.0	11.4	3.7	39.5	5.4	4.2	1.8	
1.day	1.8	10.0	6.8	2.3	33.9	2.9	3.1	0.7	
2.day	2.4	10.0	7.5	2.6	36.4	3.2	3.4	0.9	
3.day	2.6	10.0	11.6	5.6	33.4	5.6	4.5	1.6	

## CHAPTER 4

### CONCLUSION

In this study, we investigated unfunctionalized CT SAMs (M1, M9) and carboxylic group functionalized CT SAMs (M1C, M9C) as well as their corresponding mixed SAMs on template stripped gold surfaces. Wetting properties of the SAMs were studied by using contact angle (CA) measurements. In mixed SAMs, surface fraction of M1 was found to be higher than its solution fraction in the M1:M1C and M1:M9C mixtures which indicates the dominant component on the surface to be M1. Similar behavior was also observed for M9 such that surface fraction of M9 was higher than its solution fraction in the M9:M1C and M9:M9C mixtures indicating the dominance of M9 molecules on the surface. In replacement experiments, M1 molecules were found to replace more M9C molecules on template stripped gold surface. Replacement experiments of CT SAMs on silver surface were also performed. It was found that M9C molecules bind to silver surfaces through carboxylic groups rather than the thiol group. Interestingly, both on gold and silver surfaces keeping M1C films in M9 solution decreases the contact angles significantly which hints to a special interaction between M1C on surface and M9 in solution. AFM imaging of the surfaces were particularly difficult due to presence of carboxyl groups. Nevertheless, for all the studied SAMs homogeneous morphology with no significant phase separation and average roughness of about 0.3 nm was measured. In addition, XPS was used to analyze surface composition. We observed that, the intensity ratio of carboxyl group increase over time in M1 films kept in M9C solution, indicating replacement of M1 with M9C on the gold surface in agreement with the contact angle measurements. Overall, it can be concluded that unfunctionalized CTs bind to gold surface with a higher affinity than functionalized CTs. Though, we initially were hoping/thinking that the hydrogen bonding interactions between carboxyl groups could yield more

ordered and strongly adsorbed SAMs, the actual case seems to be just the opposite due to the extra steric demands in the functionalized SAMs imposed by the carboxyl groups.

## REFERENCES

- [1] Gaines, G. L., *J. Colloid. Inter. Sci.*, 149 (1) (1991).
- [2] L. C. F. Blackman and M. J. S. Dewa. *J. Chem. Soc.*, 35 (162) (1957).
- [3] W. Biglow.; D. Pickett.; W. Zisman. . *J. Colloid. Inter. Sci.*, 1 (1946).
- [4] K.B. Blodgett, *J. Am. Chem. Soc.*, 57 (6) (1935).
- [5] Folkers, J., Laibinis, P., & Whitesides, G. *Langmuir*, 8 (5) (1992).
- [6] Laibinis, P. E.; Bain, C. D.; Whitesides, G. M. *J. Phys. Chem.*, 95 (18) (1991).
- [7] Zwahlen, M.; Tosatti, S.; Textor, M.; Hähner, G. *Langmuir*, 18 (10) (2002).
- [8] Xia, Y.; Kim, E.; Mrksich, M.; Whitesides, G. M. *Chem. Mater.*, 8 (3) (1996).
- [9] Tosatti, S.; Michel, R.; Textor, M.; Spencer, N. D. *Langmuir*, 18 (9) (2002).
- [10] Schreiber, F. *Prog. Surf. Sci.*, 65 (5–8) (2000)
- [11] Schlotter, N. E.; Porter, M. D.; Bright, T. B.; Allara, D. L. *Chem. Phys. Lett.*, 132 (1) (1986)
- [12] S. Kim, G. Y. Choi, A. Ulman, and C. Fleischer, *Langmuir* 13, 6650 (1997).
- [13] S. Kidoaki and T. Matsuda, *Langmuir* 15, 7639 (1999).
- [14] J. P. Folkers, P. E. Laibinis, and G. M. Whitesides, *Langmuir* 8, 1330 (1992).
- [15] J. P. Folkers, P. E. Laibinis, G. M. Whitesides, and J. Deutch, *J. Phys. Chem.* 98, 563 (1994).
- [16] S. J. Stranick, A. N. Parikh, T. Y.-T. Tao, D. L. Allara, and P. S. Weiss, *J. Phys. Chem.* 98, 7636 (1994).
- [17] H. S. Onherr, H. Ringsdorf, M. Jaschke, H.-J. Butt, E. Bamberg, H. Allison, and S. D. Evans, *Langmuir* 12, 3898 (1996).

- [18] L. L. Bertilsson, B., *Langmuir* 9, 141 (1993).
- [19] A. Ulman, *Chem. Rev* 96, 1533 (1996).
- [20] G. L. J. Gaines, Interscience, New York, (1996).
- [21] K. L. Prime and G. M. Whitesides, *Science* 252, 1164 (1991).
- [22] L. Häußling, W. Knoll, H. Ringsdorf, F.-J. Schmitt, and J. Yang, *Makromol. Chem. Macromol. Symp.* 46, 145 (1991).
- [23] R. K. Singhvi, A. Kumar, G. P. Lopez, G. N. Stephanopoulos, D. I. C. Wang,
- [24] G. M. Whitesides, and D. E. Ingber, *Science* 264, 696 (1994).
- [25] M. J. Wirth, R.W.P. Fairbank, and H. O. Fatunmbi, *Science* 275, 44 (1997).
- [26] J. Lahiri, L. Isaacs, B. Grzybowski, J. D. Carbeck, and G. M. Whitesides, *Langmuir* 15, 7186 (1999).
- [27] N. Higashi, M. Takahashi, and M. Niwa, *Langmuir* 16, 1793 (2000).
- [28] G. B. Sigal, C. Bamdad, A. Barberis, J. Strominger, and G. M. Whitesides, *Anal. Chem.* 68, 490 (1996).
- [29] F. Malem and D. Mandler, *Anal. Chem.* 65, 37 (1993).
- [30] J. J. Gooding, V. G. Praig, and E. A. Hall, *Anal. Chem.* 70, 2396 (1998).
- [31] L. Sun, L. L. J. Kepley, and R. M. Crooks, *Langmuir* 10, 3675 (1994).
- [32] H. C. Yang, D. L. Dermody, C. J. Xu, A. J. Ricco, and R. M. Crooks, *Langmuir* 12, 726 (1996).
- [33] R. C. Sabapathy and R. M. Crooks, *Langmuir* 16, 1777 (2000).
- [34] R. P. Andres, T. Bein, M. Dorogi, S. Feng, J. I. Henderson, C. P. Kubiak, W. Mahoney, R. G. Osifchin, and R. Reifengerger, *Science* 272, 1323 (1996).

- [35] M. A. Reed, C. Zhou, C. J. Muller, T. P. Burgin, and T. J.M., *Science* 278, 25 (1997).
- [36] L. A. Bumm, J. J. Arnold, M. T. Cygan, T. D. Dunbar, T. P. Burgin, L. Jones, D. L. Allara, J. M. Tour, and P. S. Weiss, *Science* 271, 1705 (1996).
- [37] G. Leatherman, E. N. Durantini, D. Gust, T. A. Moore, A. L. Moore, S. Stone, Z. Zhou, P. Rez, Y. Z. Liu, and S. M. Lindsay, *J. Phys. Chem. B* 103, 4006 (1999).
- [38] C. E. D. Chidsey, *Science* 251, 919 (1991).
- [39] S. B. Sachs, S. P. Dudek, R. S. Hsung, L. R. Sita, J. F. Smalley, M. D. Newton, S. W. Feldberg, and C. E. D. Chidsey, *J. Am. Chem. Soc.* 119, 10563 (1997).
- [40] L. A. Bumm, J. J. Arnold, T. D. Dunbar, D. L. Allara, and P. S. Weiss, *J. Phys. Chem.* 103, 8122 (1999).
- [41] A. Ulman, S. D. Evans, Y. Shnidman, R. Sharma, J. E. Eilers, and J. C. Chang, *J. Am. Chem. Soc.* 113, 1499 (1991).
- [42] A. Berman, S. Steinberg, S. Campbell, A. Ulman, and J. Israelachvili, *Tribol. Lett.*, 43 (1998).
- [43] Azzam, Waleed., *Phys. Chem, I* (2003).
- [44] Watcharinyanon, S., Doctoral dissertation, Karlstads universitet, (2008).
- [45] H. A. Biebuyck and G. M. Whitesides, *Langmuir* 9, 1766 (1993).
- [46] J. Gottschalck and B. Hammer, *J. Chem. Phys.* 116, 784 (2002).
- [47] T. Hayashi, Y. Morikawa, and H. Nozoye, *J. Chem. Phys.* 114, 7615 (2001).
- [48] A. Dhirani, R. W. Zehner, R. P. Hsung, P. Guyot-Sionnest, and L.R. Sita, *J. Am. Chem. Soc.* 118, 3319 (1996).
- [49] A. I. Kitaigorodskii, Consultants Bureau, New York, 177 (1959).
- [50] S. Garoff, *Proc. Natl. Acad. Sci. U.S.A.* 84, 4129 (1987).

- [51] I. Langmuir, J. Chem. Phys. 1, 756 (1933).
- [52] H. T. J. Epstein, Colloid. Chem. 54, 1053 (1950).
- [53] S. A. Safran, M. O. Robbins, and S. Garoff, Phys. Rev. A 33, 2188 (1986).
- [54] A. Ulman, N. Tillman, and J. Eilers, Langmuir 5, 1147 (1989).
- [55] H.-J. Himmel, A. Terfort, and C. Wöll, J. Chem. Phys. 120, 12069 (1998).
- [56] N. Tillman, A. Ulman, and T. L. Penner, Langmuir 5, 101 (1989).
- [57] S. D. Evans, R. Sharma, and A. Ulman, Langmuir 7, 156 (1991).
- [58] C. P. Collier, E. W. Wong, M. Belohradsky, F. M. Raymo, J. F. Stoddart, P. J. Kuekes, R. S. Williams, and J. R. Heath, Science 1999, 391 (1999).
- [59] C. Zhou, M. R. Deshpande, M. A. Reed, L. Jones, and J. M. Tour, Appl. Phys. Lett. 71, 611 (1997).
- [60] G.E. Poirier, M.J. Tarlov, and H.E. Rushmeier, Langmuir, 10 (10), (1994).
- [61] G.E. Poirier and E.D. Pylant, Science, 272 (5265), (1996).
- [62] G. Poirier, Chem. Rev., 97 (4), (1997).
- [63] N. Camillone, T.Y.B. Leung, P. Schwartz, P. Eisenberger, and G. Scoles, Langmuir, 12 (11), (1996).
- [64] S. W. Han, C. H. Kim, S. H. Hong, Y. K. Chung, and K. Kim, Langmuir 15, 1579 (1999).
- [65] K. Tamada, J. Nagasawa, F. Nakanishi, K. Abe, T. Ishita, M. Hara, and W. Knoll, Langmuir 14, 3264 (1998).
- [66] R. Wang, T. Iyoda, L. Jiang, K. Hashimoto, and A. Fujishima, Chem. Lett. 47, 1005 (1996).

- [67] W. B. Caldwell, D. J. Campbell, K. Chen, B. R. Herr, C. A. Mirkin, A. K. Malik, P. Dutta, and K. G. Huang, *J. Am. Chem. Soc.* 117, 6071 (1995).
- [68] D. Käfer, A. Bashir, and G. Witte, *J. Phys. Chem. C*, 111 (28) (2007).
- [69] M.A. Reed, C. Zhou, C.J. Muller, T.P. Burgin, and J.M. Tour, *Science*, 278 (5336) (1997).
- [70] A. Ulman, *Chem. Rev.*, 96 (4) (1996).
- [71] O. Dannenberger, K. Weiss, H.J. Himmel, B. Jager, M. Buck, and C. Wöll, *Thin Solid Films*, 307 (1-2) (1997).
- [72] A. Wesch, O. Dannenberger, C. Wöll, J.J. Wolff, and M. Buck, *Langmuir*, 12 (22) (1996).
- [73] Rajalingam, Ketheeswari, *ChemPhysChem* 8.5, 657-660 (2007).
- [74] C.A. Alves and M.D. Porter, *Langmuir*, 9 (12) (1993).
- [75] M.W. Tsao, J.F. Rabolt, H. Schonherr, and D.G. Castner, *Langmuir*, 16 (4) (2000).
- [76] C.D. Bain, H.A. Biebuyck, and G.M. Whitesides, *Langmuir*, 5 (3) (1989).
- [77] M. Sprik, E. Delamarche, B. Michel, U. Roethlisberger, M.L. Klein, H. Wolf, and H. Ringsdorf, *Langmuir*, 10 (11) (1994).
- [78] D.A. Hutt and G.J. Leggett, *Langmuir*, 13 (10) (1997).
- [79] M.J. Esplandiu, H. Hagenstrom, and D.M. Kolb, *Langmuir*, 17 (3) (2001).
- [80] J. Pflaum, G. Bracco, F. Schreiber, R. Colorado, O.E. Shmakova, T.R. Lee, G. Scoles, and A. Kahn, *Surf. Sci.*, 498 (1-2) (2002).
- [81] C.D. Bain, E.B. Troughton, Y.T. Tao, J. Evall, G.M. Whitesides, and R.G. Nuzzo, *J. Am. Chem. Soc.*, 111 (1) (1989).

- [83] J.C. Love, L.A. Estroff, J.K. Kriebel, R.G. Nuzzo, and G.M. Whitesides, *Chem. Rev.*, 105 (4) (2005).
- [84] D.I. Gittins, D. Bethell, D.J. Schiffrin, and R.J. Nichols, *Nature*, 408 (2000).
- [85] E. Blomberg, P.M. Claesson, P. Konradsson, and B. Liedberg, *Langmuir*, 22 (24) (2006).
- [86] L. Yan, C. Marzolin, A. Terfort, and G.M. Whitesides, *Langmuir*, 13 (25) (1997).
- [87] G. Binnig, H. Rohrer, C. Gerber, and E. Weibel, *App.Phy.Let.*, 40 (2) (1982).
- [88] M.L. Carot, V.A. Macagno, P. Paredes-Olivera, and E.M. Patrito, *J. Phys. Chem. C*, 111 (11) (2007).
- [89] J. Tersoff, D.R. Hamann, *Phy. Rev. Let.*, 50 (25) (1983).
- [90] J. Tersoff, D.R. Hamann, *Phy. Rev. B*, 31 (2) (1985).
- [91] J. Bardeen, *Phy. Rev. Let.*, 1961. 6 (2) (1961).
- [92] Pohl, Dieter W, *IBM Journal of Research and Development* 30.4: 417-427 (1986).
- [93] Azzam, Waleed. *Phy. Chem.*, I (2003).
- [94] M.A. Habib and J.O.M. Bockris, *J. Elec. Chem.*, 180 (1-2) (1984).
- [95] Parksystems.com., *AFM*, (2019).
- [96] HORIBA. *Spectroscopic Ellipsometry*, (2019).
- [97] Yavuz, A.; Sohrabnia, N.; Yilmaz, A.; Danişman, M. F. *Appl. Surf. Sci.* 413 (2017).
- [98] Sohrabnia, Nima. MS thesis. MIDDLE EAST TECHNICAL UNIVERSITY (2017).

- [99] Hohman, J. N.; Zhang, P.; Morin, E. I.; Han, P.; Kim, M.; Kurland, A. R.; McClanahan, P. D.; Balema, V. P.; Weiss, P. S. *ACS Nano*. 3 (3) (2009).
- [100] P. Sherwood, *Data Analysis in X-ray Photoelectron Spectroscopy*. J. Wiley and Sons Ltd, New York, NY (1990).
- [101] Bashir, Asif. Doctoral thesis (2008).
- [102] Thomas, J. C.; Boldog, I.; Auluck, H. S.; Bereciartua, P. J.; Dušek, M.; Macháček, J.; Bastl, Z.; Weiss, P. S.; Baše, T. *Chem. Mater.* 27 (2015).
- [103] C. Yan, M. Zharnikov, A. Golzhauser, M. Grunze, *Langmuir* 16, 6208 (2000)
- [104] Mete, E.; Yılmaz, A.; Danişman, M. F. *Phys. Chem. Chem. Phys.* 18 (18) (2016).
- [105] <https://www.quora.com/How-does-atomic-force-microscopy-work> (2020).
- [106] Hsu, C.; Marcus, R. J. *Chem. Phys.* , 106 (2) (1997).



## APPENDICES

### A. Raw data of XPS measurements

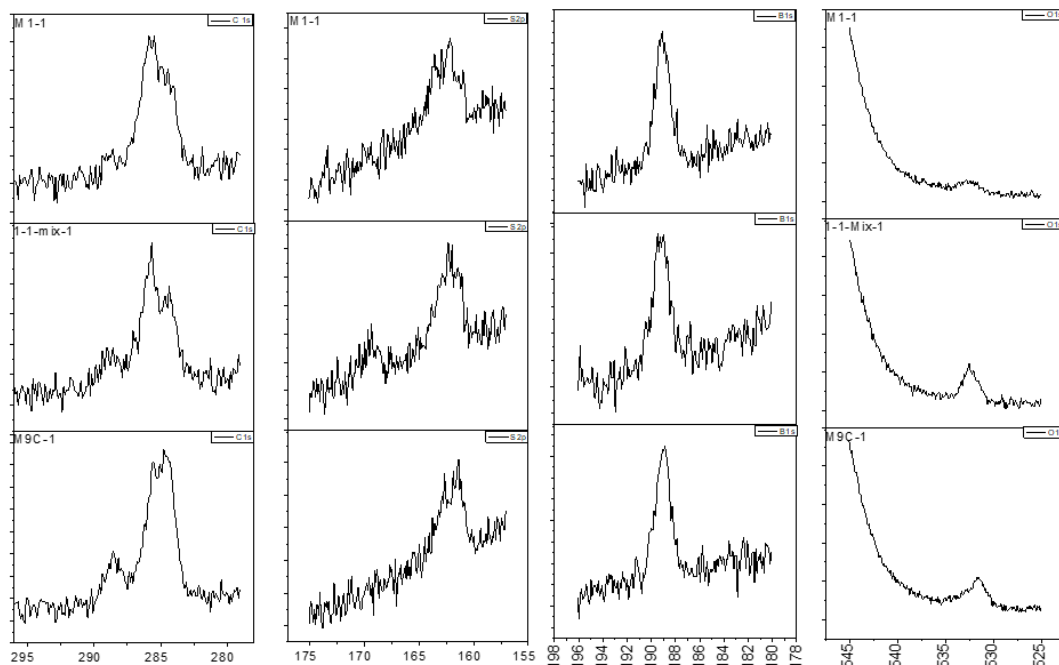


Figure 0-1 Raw data of M1, 1:1-Mix, M9C samples.

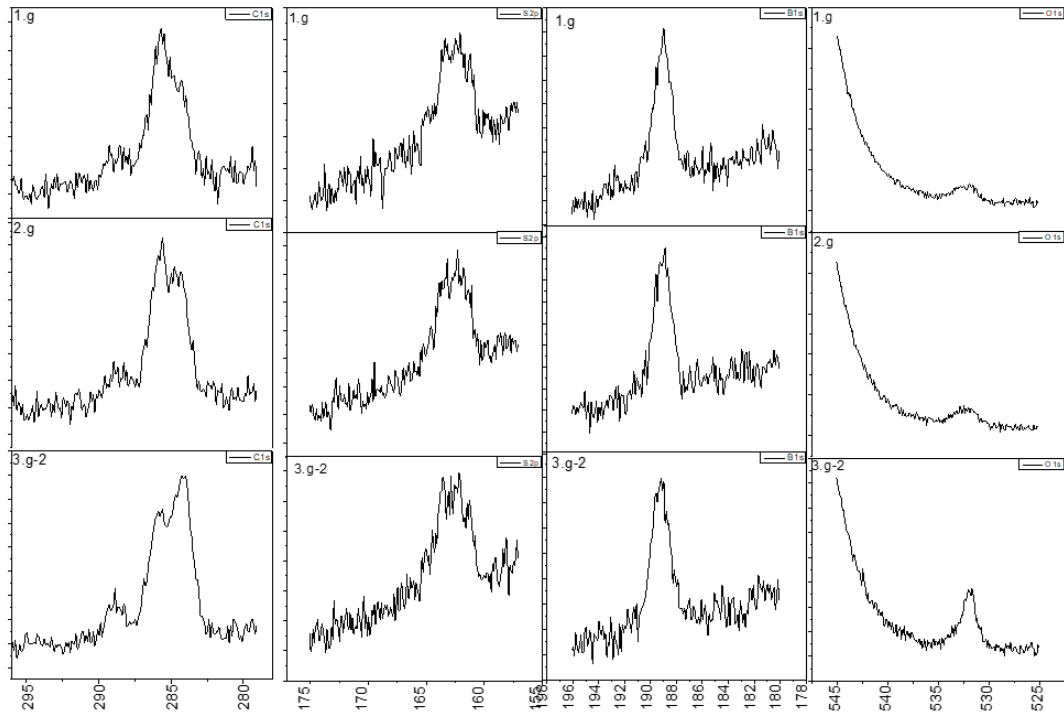


Figure 0-2 Raw data of M1 films kept in M9C solution 1.d,2.d, 3.d samples